The Route from Green H$_2$ Production through Bioethanol Reforming to CO$_2$ Catalytic Conversion: A Review

Eugenio Meloni *, **Marco Martino**, **Giuseppina Iervolino**, **Concetta Ruocco**, **Simona Renda**, **Giovanni Festa** and **Vincenzo Palma**

Department of Industrial Engineering, University of Salerno, Via Giovanni Paolo II 132, 84084 Fisciano, Italy; mamartino@unisa.it (M.M.); giiervolino@unisa.it (G.I.); cruocco@unisa.it (C.R.); srenda@unisa.it (S.R.); gifesta@unisa.it (G.F.); vpalma@unisa.it (V.P.)
* Correspondence: emeloni@unisa.it

Abstract: Currently, a progressively different approach to the generation of power and the production of fuels for the automotive sector as well as for domestic applications is being taken. As a result, research on the feasibility of applying renewable energy sources to the present energy scenario has been progressively growing, aiming to reduce greenhouse gas emissions. Following more than one approach, the integration of renewables mainly involves the utilization of biomass-derived raw material and the combination of power generated via clean sources with conventional power generation systems. The aim of this review article is to provide a satisfactory overview of the most recent progress in the catalysis of hydrogen production through sustainable reforming and CO$_2$ utilization. In particular, attention is focused on the route that, starting from bioethanol reforming for H$_2$ production, leads to the use of the produced CO$_2$ for different purposes and by means of different catalytic processes, passing through the water–gas shift stage. The newest approaches reported in the literature are reviewed, showing that it is possible to successfully produce "green" and sustainable hydrogen, which can represent a power storage technology, and its utilization is a strategy for the integration of renewables into the power generation scenario. Moreover, this hydrogen may be used for CO$_2$ catalytic conversion to hydrocarbons, thus giving CO$_2$ added value.

Keywords: catalysis; bioethanol; reforming; water–gas shift; CO$_2$ methanation; carbon capture and storage; carbon capture and utilization; catalytic conversion of CO$_2$

1. Introduction

Today, climate change is widely recognized as the greatest immediate threat to Earth's ecosystem. At the COP21 meeting (held in December 2015), 197 countries proposed an agreement to navigate the impacts of climate change by limiting their greenhouse gas (GHG) emissions. In this way, the aim is to limit the global temperature rise to 2 °C, with an aspiration of 1.5 °C. By setting out a practical pathway to fulfill the United Nation's Sustainable Development Goals, COP21 represents the first tangible international move towards a low-carbon future [1]. The over 40 billion tons per year of anthropogenic carbon emissions as CO$_2$ (largely originating from the combustion of fossil fuels) plays a key role in the overall temperature rise that is actually measured [2]. In 2018, the main sectors contributing to these emissions were: (i) electricity and heat production (~13.9 billion) tons, (ii) transport (~8.2 billion tons), (iii) manufacturing industries and construction (~6.2 billion tons), and (iv) buildings (2.9 billion tons) [3]. Since fossil fuels are still responsible for 80% of the global primary production, a 60% reduction in carbon emissions from both energy and industrial sectors is mandatory for reaching the COP21 climate change target [4]. Therefore, the shift towards low-carbon technologies needs to be accelerated; otherwise, the target cannot be reached. In this sense, the combined use of renewable energies (for example, solar, wind, and clean fuels such as H$_2$) and

advanced energy storage devices are considered very promising "longer-term" solutions to realize a low-carbon world. However, rapidly reducing the consumption of fossil fuels in developing countries is considered a much greater challenge compared to their developed counterparts [5]. These last strategies, which aim at limiting CO_2 emissions by acting directly at the emission source (e.g., flue gases associated with power/industry sectors), may be considered an anticipated short- to mid-term solution to atmospheric carbon reduction. Carbon capture and storage (CCS) is considered the "priority breakthrough technology" by the European Commission, which, in their Green Deal, encouraged new funding within the post-COVID-19 recovery package [6]. Different feasible roadmaps (Figure 1) are possible, and among them, H_2 seems to have extraordinary potential to become the most widely used commercially viable clean fuel of the future [3].
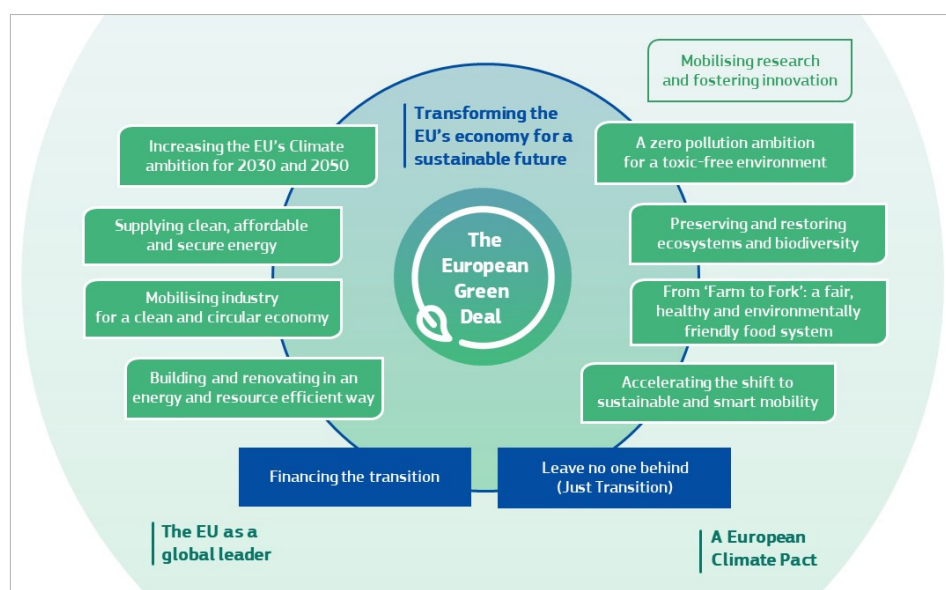

Figure 1. The European Green Deal.

In fact, the use of H_2 in the energy and power sectors can be considered one of the most practical pathways in carbon emission reduction. More recently, the European Commission stated that hydrogen would play a major role in the economic recovery of post-COVID-19 EU countries [7]. However, although H_2 is considered a low-carbon fuel, the main processes leading to its production (especially the steam reforming process) are characterized by a high amount of carbon emissions. Alternative processes for hydrogen production include electrolysis, thermolysis, biomass gasification, biocatalysis, and fermentation [3]. The adopted process for H_2 production leads to the identification of three different categories: (i) gray hydrogen (i.e., via reforming fossil fuels), (ii) blue hydrogen (i.e., with carbon captured, utilized, or stored—CCUS), and (iii) green hydrogen (i.e., via the utilization of a renewable feedstock as well as renewable energy sources, such as wind and solar, nuclear, geothermal, biomass, and hydropower) [2]. Depending on the production route, total carbon emissions could be considerably reduced [2]. In this review, attention is focused on the route that, starting from bioethanol reforming for H_2 production, leads to the use of the produced CO_2 for different purposes and by means of different catalytic processes. Therefore, in the different sub-sections, the newest approaches in bioethanol reforming, water–gas shift (WGS), and CO_2 catalytic conversion are described, aiming to address the scientific community's interest in the use of catalysis for sustainable and green processes.

2. Catalysis for Sustainable Processes

At present, a significant challenge in which the chemical and allied industries are involved can be identified: the transition to greener, more sustainable manufacturing processes that efficiently use raw materials [8]. This transition can be realized if the

traditional concepts of process efficiency, focusing on chemical yield, are replaced by approaches in which the main importance is assigned to replacing fossil resources (oil, coal, and natural gas) with renewable raw materials. In this way, the targets of limiting waste and avoiding the use of toxic and/or hazardous substances may also be reached [9]. Another attractive approach is the valorization of waste biomass, which is currently incinerated or goes to the landfill [10]. The bio-based economy involves cross-disciplinary research at the interface of biotechnology and chemical engineering, focusing on the development of green, chemo- and biocatalytic technologies for waste biomass conversion to biofuels, chemicals, and bio-based materials [11]. In particular, the utilization of biomass impacts different fields. On the one hand, biomass fermentation allows the obtainment of fuels such as bioethanol, which can be employed as such or can be further valorized by its subsequent conversion into hydrogen, which is widely seen as the energy vector of the future. On the other hand, bioethanol is not the only product of biomass fermentation; indeed, a considerable amount of CO_2 is contextually generated. Therefore, green chemistry cannot limit its actions to the obtainment and conversion of bioethanol but should also be capable of utilizing the produced carbon dioxide in order to be a carbon-free technology. Carbon dioxide utilization is a newborn topic in the research context, but the widely shared ideal is its catalytic conversion into hydrocarbons and alcohol, mainly through hydrogenation reactions. The obtained products can be further employed as chemicals and/or as fuels. Hence, starting from the fermentation of waste biomass, it is possible to obtain two valuable components: bioethanol, which can be upgraded to green hydrogen through reforming and water–gas shift processes, and carbon dioxide, which can be converted into substitute natural gas, other green fuels, or alcohols via hydrogenation. A schematic representation of the discussed connections among processes is displayed in Figure 2.
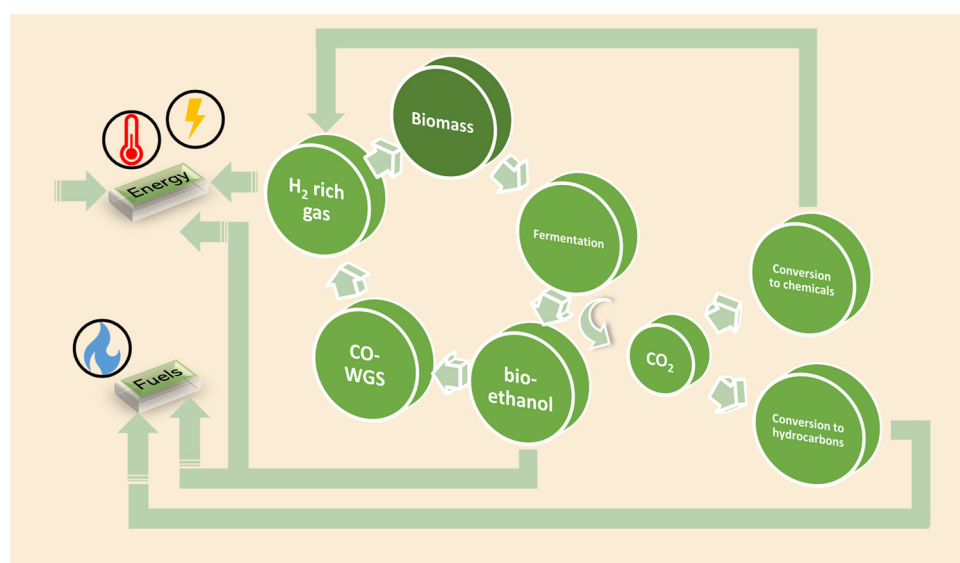

Figure 2. From biomass to hydrogen and fuels: schematic overview.

Therefore, in the following sub-sections, green H_2 production from bioethanol reforming is critically reviewed, and details regarding further purification through WGS and the consequent CO_2 catalytic conversion are provided.

2.1. H_2 Production from Renewables: Bioethanol Reforming

In the context of sustainable energy generation, bioethanol produced from biomass has been regarded as one of the cleanest and greenest sources of electricity through the conversion of the derived hydrogen in fuel cell devices [12]. In fact, when renewable sources are used for hydrogen generation, fuel cell operation avoids greenhouse gas emissions [13]. Moreover, liquid fuels such as bioethanol are very interesting for on-site hydrogen generation in small-scale fuel reformers devoted to both portable and mobile power source

applications [14]. Among the many non-thermal as well as thermo-chemical processes available for making H_2 from bioethanol, the steam reforming process attracts the interest of the scientific community thanks to the high H_2 yield and ethanol conversion rate. Although the only expected products of ethanol reforming are H_2 and carbon oxides, the reaction mechanism is quite complex, and different pathways, including ethanol decomposition, dehydrogenation to acetaldehyde, and dehydration to ethylene, may also occur. Such reactions are responsible for reduced hydrogen yield and may accelerate the occurrence of deactivation phenomena. Ethylene, for example, can be subsequently polymerized to coke, which is deposited on the catalyst active sites, causing a pronounced deterioration in performance [15]. In this regard, the product selectivity recorded during ethanol reforming can be tuned by selecting the proper operating conditions (feed composition, temperature, and pressure, as well as contact time) and choosing a suitable catalytic system [16,17].

2.1.1. Catalytic Formulations

Different catalytic formulations have been investigated for H_2 production via the bioethanol reforming route, and various strategies have been proposed for the enhancement of H_2 production yield as well as catalyst resistance to deactivation [18]. Due to the extremely large number of works focused on the bioethanol reforming topic, the present review is dedicated to papers published in the last two years. In particular, in view of the direct utilization of bioethanol from biomass for reforming applications, issues related to the durability of catalysts are becoming even more important subjects. In fact, raw bioethanol contains several organic and inorganic impurities, which were shown to strongly affect the catalyst deactivation rate due to coke formation during steam reforming [19,20]. For example, it was reported [21] that the carbon formation rate increases by almost 15% during ethanol steam reforming over a $RhPt/CeO_2-SiO_2$ catalyst at 700 °C when the reacting stream is switched from synthetic ethanol to glucose bioethanol.

From a catalyst stability standpoint, efforts made in the recent literature are mainly devoted to the development of innovative catalysts with improved active species–support interactions as well as enhanced metal particle dispersion, which are expected to result in the easier oxidation of carbonaceous deposits that eventually form on the catalyst surface. In fact, by modifying the metal, the support, or both, it is possible to stop carbon formation prior to and subsequent to deposition [22]. In this regard, the influence of redox/basic supports has been widely investigated in order to suppress coke formation and side reactions [23]. Moreover, different parameters, including the metal loading, the preparation method, and the addition of promoters, were shown to affect catalyst resistance to deactivation.

Ferreira et al. [24] investigated the influence of cobalt content (in the interval 5–15 wt%) on the performance of a $Co/La_2O_3–SiO_2$ catalyst for ethanol steam reforming at 500 °C, 1 atm, and a H_2O/C_2H_5OH ratio of 5. The characterization measurements performed on the spent catalysts revealed that the samples with the lowest Co loading promoted the formation of carbon nanotubes, with a subsequent reduction in ethanol conversion and hydrogen yield. Conversely, for a cobalt content of 15 wt%, only the formation of amorphous carbon was observed, which was not able to modify the electronic environment of the catalyst, thus assuring a constant hydrogen yield (of 3.5 $mol_{H2} \cdot mol_{C2H5OH,fed}^{-1}$) with time-on-stream. For a nickel catalyst supported on hydrocalumite, the impact of Ni loading was studied in the same range as above (5–15 wt%) [25]: a decrease in the Ni particle size with the increase in the metal content was found as a consequence of an improvement in the specific surface area of the final sample upon the introduction of more Ni. Moreover, the samples with the smallest Ni particle dimensions displayed more pronounced interaction with the catalytic support, with enhanced total basicity and higher activity as well as stability for ethanol steam reforming.

Efimov et al. [26] demonstrated how the catalyst preparation method could affect the dimensions of metallic Co and Ru particles supported on highly porous carbon and, as a consequence, the catalyst performance during ethanol reforming. The samples were

prepared starting from polyacrylonitrile, which, after impregnation with the active species, was pyrolyzed at 800 °C under IR radiation. This synthesis procedure allowed the formation of a structure containing metal–carbon nanocomposites with a reduced tendency towards nanoparticle agglomeration. During stability tests performed at 500 °C, 1 atm, and a H_2O/C_2H_5OH ratio of 3, the highest ethanol conversion and H_2 yield were recorded for the bimetallic Co–Ru sample, for which the deposition of carbonaceous species only involved the catalytic support. Conversely, for the monometallic Co-based catalyst, a carbon shell also covered the cobalt nanoparticles, with a consequent deterioration in durability.

In order to improve cobalt and nickel dispersion on ceria as well as metal–support interactions, the influence of the use of organic and inorganic precursors, different impregnation solutions, and the addition of organic precursors during the preparation of Ni/CeO_2 and Co/CeO_2 was investigated. When cobalt or nickel acetate was dissolved in the ammonia solution, a reduction in the specific surface area and in the growth of the metals particles was observed. The use of acetates instead of nitrates as Ni or Co precursors also caused a slight increase in nickel as well as cobalt particles. Moreover, better dispersion of metal particles on the catalytic support was achieved by adding citric acid to the aqueous solution of nitrate salts. Concerning the influence of the metal particle size on catalyst stability, the same authors found that, as carbon nucleation requires relatively large domains of flat terraces or larger ensemble sizes, the terrace atoms are involved in catalyst deactivation under ethanol steam reforming conditions. Conversely, an increase in the fraction of edges and corners, which indicates better dispersion and stronger metal–oxide interactions between metal and ceria, was found to enhance the transfer of oxygen and thus improve the oxidation of carbon formed on the catalyst surface during stability tests. Figure 3 summarizes the dependence of (a) ethanol conversion and (b) H_2 selectivity on metal particle sizes for the Ni and Co series in stability tests performed at 420 °C, atmospheric pressure, and $H_2O/C_2H_5OH = 12$ for 3 h and demonstrates that the catalyst performance was negatively affected by an increase in particle dimensions.
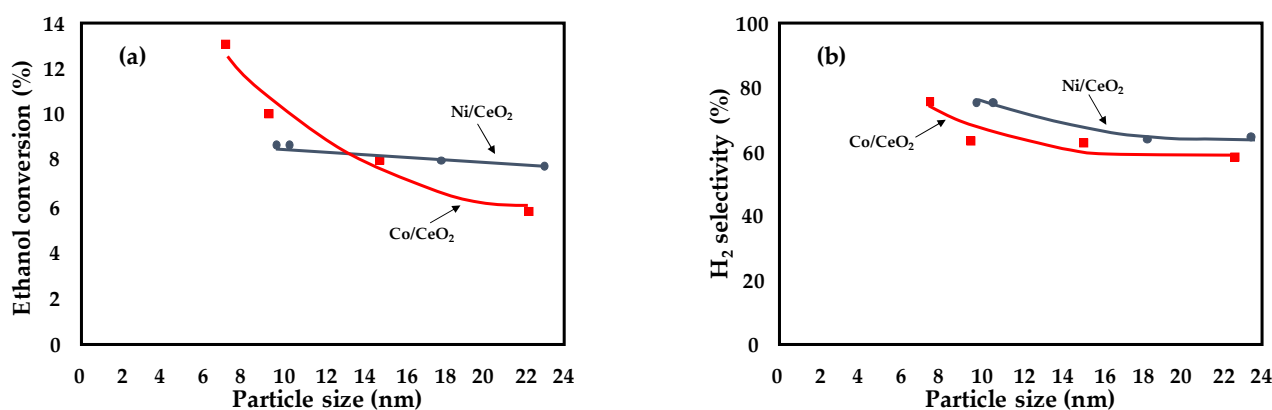

Figure 3. Catalytic performance of Co- and Ni-supported CeO_2 samples as a function of the metal particle size. Adapted from [27]; T = 420 °C; P = 1 atm; $H_2O/C_2H_5OH = 12$; GHSV = 1,286,000 mL·g^{-1} h^{-1}. (**a**) ethanol conversion and (**b**) H_2 selectivity vs metals particle size.

For Ni/CeO_2 catalysts, Pizzolitto et al. [28] demonstrated that the use of impregnation instead of microemulsion as the preparation method allowed the synthesis of a more reducible sample (with higher oxygen mobility) and allowed obtaining a more homogeneous Ni particle size distribution. As a result, the catalyst prepared via the microemulsion route displayed a considerable extent of deactivation during stability tests performed at 500 °C, 1 atm, and $H_2O/C_2H_5OH = 5.9$ due to the quite high proportion of active sites covered by coke. On the other hand, when a Ni/Al_2O_3 catalyst was prepared via coprecipitation from a $NiAl_2O_4$ spinel [29], only carbon nanotubes were observed over the used catalyst after 48 h of time-on-stream at 500 °C, 1 atm, and $H_2O/C_2H_5OH = 3$. Carbon nanotubes formed

a tangle of hollow carbon fibers with a porous structure, allowing reactants and products to diffuse and reach catalytic sites, which resulted in high catalyst stability compared to other Ni/Al_2O_3 samples synthesized from other routes.

Another promising strategy to properly address catalyst selectivity and improve resistance to deactivation is related to the addition of small quantities of various elements (defined as promoters) to modify the support or in the final step of catalyst preparation. For example, Musso et al. [30] modulated the performance of a $Ni/Me_2Zr_2O_7$ catalyst by adding Me = Y or La (with a Me/Zr ratio of 1:1) in the support structure. The samples were prepared by the sol–gel technique and calcined at different temperatures between 700 and 950 °C. The use of Y instead of La led to the formation of a higher number of oxygen vacancies, with an improvement in terms of metal–support interactions. In particular, the Y-based catalyst calcined at 950 °C displayed no apparent deactivation during ethanol reforming tests performed at 650 °C, 1 atm, and H_2O/C_2H_5OH = 9. For a $Rh/ZrO_2\text{-}La_2O_3$ catalyst [31], the addition of 15% CeO_2 to the support markedly enhanced the catalyst performance at 400 °C, 1 atm, and H_2O/C_2H_5OH = 3: ceria, due to its high oxygen mobility, was able to effectively promote CO conversion to CO_2 through the water–gas shift reaction. Furthermore, CeO_2 enhanced the coke resistance of the catalyst and, after 4 h of time-on-stream tests, the carbon formation rate was reduced by almost 90% compared to the catalyst supported on ZrO_2–La_2O_3. On the other hand, for a $Rh/LaAl_2O_3$ catalyst [32], the introduction of 10% ceria into the structure resulted in an evident reduction in carbon accumulation in time-on-stream tests performed at 500 °C, 1.2 atm, and H_2O/C_2H_5OH = 5 compared to the CeO_2-free sample. However, ceria also caused the partial oxidation of Rh° to the less active Rh^{3+} species; consequently, after 14 h of testing, a decreasing trend in both ethanol conversion and H_2 yield was observed. Boudadi et al. [33] observed that La addition (10 wt%) to a Ni/Al_2O_3 catalyst weakened the strength of the Brønsted sites of the sample; in the absence of strong acidic sites that can retain ethylene, it can be easily desorbed, thus disfavoring the polymerization mechanism. By improving lanthana dispersion, this effect can be enhanced due to its slightly basic properties.

The addition of Cs to a zirconia support for a Pt/ZrO_2 catalyst was shown to improve the catalyst activity towards the ethanol decarboxylation route over the decarbonylation pathway, thus enhancing the hydrogen production rate [34]: a cesium loading of 2.9 wt% was able to stave off decarbonylation almost completely; under the same operating conditions (450 °C, 1 atm, and H_2O/C_2H_5OH = 9), the amount of sodium that is required to achieve the same effect is almost 80% higher [35]. Similarly, the contribution of the latter route can be augmented by promoting monoclinic zirconia with 3.1 wt% K or 6.7 wt% Rb [36].

Recently, with the aim of enhancing the performance of Ni catalysts for ethanol reforming, the addition of small quantities of a second metal as a promoter has been widely investigated. Matus et al. [37] performed oxidative steam reforming of ethanol in the presence of $Ni/Ce_{0.8}La_{0.2}0_{1.9}$ catalysts promoted by Pt, Pd, Rh, and Re (with a molar ratio of noble metal/Ni = 0.003–0.012). During stability tests performed at 500 °C, 1 atm, H_2O/C_2H_5OH = 3, and O_2/C_2H_5OH = 0.5, complete ethanol conversion was recorded for all of the promoted samples: the addition of the noble metal, in fact, improved the dispersion of the Ni-supported nanoparticles, and the formation of a Ni–noble metal alloy improved the catalyst resistance to oxidation, sintering, and coking. The best results were recorded for the 10Ni-0.4Re catalyst, which displayed a H_2 yield of 65% at 600 °C. For NiAl layered double hydroxides, upon Cu addition (molar ratio Ni^{2+}/Cu^{2+} = 5/1), the synergistic effect between nickel and copper increased the ethanol conversion rate, resulting in complete values at 500 °C, 1 atm, and H_2O/C_2H_5OH = 3. On the other hand, the presence of Cu atoms on the surface of Ni particles allowed eliminating many Ni atom aggregates that are normally required for carbon deposition, which suppressed coking phenomena. Moreover, by adding Mg (molar ratio $Mg^{2+}/(Ni^{2+}+Cu^{2+})$ = 2/1), the acidic sites of the catalyst were neutralized, and no ethylene (product of ethanol dehydration) was obtained [38]. For a Rh/SiO_2 catalyst promoted by Fe [39], the strong

metal–oxide interactions between the formed Fe–Rh alloy and the FeO_x phases inhibited the acetaldehyde decomposition pathway, which is responsible for carbon monoxide as well as methane formation. Conversely, the rate of the ethanol steam reforming reaction is enhanced, with the formation of mainly CO_2 and H_2. The modification of a $Ni/MgAl_2O_4$ catalyst through the addition of Fe (molar ratio between Ni and Fe of 1/1) led to the formation of a Ni–Fe alloy, which, at a steam-to-ethanol ratio of 4, was gradually oxidized by water to generate a Ni-rich alloy and Fe_2O_3 species [40]. Moreover, within the Ni–Fe alloy, a particular electronic transfer was established that weakened CO absorption, thus inhibiting the methanation pathway. In particular, the oxidation capacity of the Fe_2O_3 species enhanced the conversion of ethoxy to acetate groups and prevented the promotion of methane formation and, at the same time, the elimination of carbonaceous species eventually deposited on the catalyst surface.

Table 1 summarizes the recent strategies put forward in order to improve active phase dispersion as well as catalyst durability. In the last year, the main routes followed to address the hot topic of ethanol reforming catalyst deactivation involved the evaluation of the effects of active metal loading, the preparation method, and the addition of promoters. In many cases, readily applicable methods (related, for example, to the utilization of a different salt precursor or the addition of small amounts of rare-earth oxides) were found to significantly improve the durability of the final catalyst.

Table 1. Different approaches found in the recent literature to enhance particle dispersion and increase catalyst stability during ethanol reforming.

Catalyst	(D [a], %) or (d [b], nm)	Experimental Results	Strategy	Ref.
Co/La_2O_3–SiO_2	d_{Co} = 6 nm	X [c] = 100% for 25 h T = 500 °C f.r. [d] = 5 W/F [e] = 3.3 10^2 g h L^{-1} CFR [f] = $1.4 \cdot 10^{-3}$ gc·gcat^{-1}·h^{-1}	Metal loading: enhancement of catalyst surface area upon the increase in metal content	[24,25]
Ni/hydrocalumite	d_{Ni} = 28 nm	X = 99% T = 550–700 °C f.r. = 6	Metal loading: enhancement of catalyst surface area upon the increase in metal content	
Co–Ru/carbon	$d_{Co\text{-}Ru}$ = 12 nm	X = 100% for 16 h T = 550 °C f.r. = 3 GHSV [g] = 89 h^{-1}	Preparation method: pyrolysis of polyacrylonitrile	[26]
Ni/CeO_2 Co/CeO_2	$d_{Co/Ni}$ = 10–22 nm	X = 8% T = 420 °C f.r = 12 GHSV = 1,286,000 mL h^{-1}·g^{-1}	Preparation method: use of acetates as salt precursors; addition of citric acid to nitrate salt precursors	[27]
Ni/CeO_2	d_{Ni} = 25 nm	X = 100% T = 500 °C f.r. = 6 W/F = 0.12 g$_{cat}$·h·mol^{-1}	Preparation method: impregnation instead of microemulsion	[28]
Ni/Al_2O_3	d_{Ni} = 50 nm	X = 100% for 48 h T = 600 °C f.r. = 3 Space time = 0.2 CFR = 0.4 gc·gcat^{-1}·h$^-$	Preparation method: coprecipitation instead of impregnation	[29]
$Ni/Me_2Zr_2O_7$	d_{Ni} = 15 nm	X = 100% for 50 h T = 650 °C f.r. = 9 GHSV = 41,000 h^{-1} CFR = 9 10^{-4} gc·gcat^{-1}·h^{-1}	Promoter: yttria addition with a Me/Zr molar ratio of 1:1	[30]
Rh/ZrO_2–La_2O_3	D_{Rh} = 29%	X = 95% for 4 h T = 500 °C f.r. = 6 W/F = 358.57 g·s·g$_{ethanol}$$^{-1}$ CFR = 2.5 10^{-4} gc·gcat^{-1}·h^{-1}	Promoter: addition of CeO_2 to the support	[31,32]

Table 1. *Cont.*

Catalyst	(D [a], %) or (d [b], nm)	Experimental Results	Strategy	Ref.
Rh/LaAl$_2$O$_3$	-	X = 100% for 24 h T = 500 °C f.r. = 5 WHSV= 10^{-3} mL·mg$_{cat}^{-1}$ min^{-1} CFR = 5.5 10^{-4} gc·gcat^{-1}·h^{-1}	Promoter: addition of CeO$_2$ to the support	
Ni/Al$_2$O$_3$	d$_{Ni}$ = 20 nm	X = 50% after 6 h T = 500 °C f.r. = 6 CFR = 1.7 10^{-2} gc·gcat^{-1}·h^{-1}	Promoter: addition of La$_2$O$_3$ to the support	[33]
Ni/Ce$_{0.8}$La$_{0.2}$O$_{1.9}$	d$_{Ni}$ = 15 nm	X = 100% T = 400 °C f.r. = 4	Promoter: Re addition to Ni instead of Pt, Pd or Rh	[37]
NiAl layered double hydroxides	d$_{Ni}$ = 11 nm	X = 100% for 18 h T = 500 °C f.r. = 3	Promoter: Cu and Mg addition (molar ratio Mg^{2+}/(Ni^{2+}+Cu^{2+}) = 2/1)	[38]
Ni/MgAl$_2$O$_4$ catalyst	dNi = 8 nm	X = 100% for 3 h T = 400 °C f.r. = 8 GHSV = 59,146 mL·g^{-1}·h^{-1}	Promoter: Fe addition with an Fe/Ni molar ratio of 1:1	[40]

[a] Metal dispersion (D, %); [b] metal particle size (d, nm); [c] ethanol conversion (X, %); [d] steam to ethanol ratio (f.r.); [e] contact time, defined as weight of the catalyst divided by the total feed flow rate (g h L^{-1}); [f] carbon formation rate, CFR; [g] gas hourly space velocity, GHSV.

From the above discussion, it is clear that the different tendencies of catalytic formulations to favor carbon formation are strictly related to the selected active species, support, and promoters, along with the chosen preparation method and the operating conditions for the activity tests. In particular, the nature of the chosen metal influences ethanol activation pathways, and metal particle sizes play a crucial role in terms of resistance to coke formation as well as oxidation [41]. In this regard, the results shown in Table 1 highlight that the prepared catalyst displays very low dimensions for metal particles (in the interval 8–50 nm); the preparation of highly dispersed catalysts allows high durability during ethanol reforming with reduced carbon formation rates.

According to the main pathway of ethanol reforming, although only CO$_2$ and hydrogen should be formed, the reaction mechanism is more complex (Table 2), and various side reactions may occur, reducing hydrogen yield and purity.

In this regard, Gu et al. [43] recently investigated the mechanism of the whole reaction pathway from ethanol to CO and, subsequently, CO$_2$ over a Rh/CeO$_2$ catalyst; this latter step is highly desired in order to reduce the impact of the downstream hydrogen purification steps. When changing the temperature from 650 to 800 °C and the steam to ethanol ratio from 2 to 6 at ambient pressure, ethanol dehydrogenation at the OH group was identified as the rate-determining step, and the CO and CO$_2$ production rate was found to be favored by temperature growth; moreover, the increase in the water molar ratio led to enhanced CO$_2$ production. On the other hand, Martinelli et al. [44] found that an interesting strategy to promote CO$_2$ formation instead of CO is the route of noble-metal-based catalyst doping via Na addition. Under selected operating conditions [45], which involved a quite diluted system and low space velocities (which means improved contact times between the catalyst and the reacting stream), at temperatures below 350 °C, the reaction mechanism did not involve carbon monoxide formation over a Cu/Al oxide catalyst.

However, from the perspective of industrial development of the ethanol reforming process, the required operating conditions may promote unwanted reaction pathways, which necessitates the use of downstream purification units (i.e., WGS reaction described in Section 2.2).

Table 2. Main pathways involved in ethanol steam reforming [42].

Reaction	Equation	Remarks
Sufficient steam supply	$C_2H_5OH + 3H_2O \leftrightarrow 6H_2 + 2CO_2$	Ideal pathway, the highest hydrogen production
Insufficient steam supply	$C_2H_5OH + H_2O \leftrightarrow 4H_2 + 2CO$ $C_2H_5OH + 2H_2 \leftrightarrow 2CH_4 + H_2O$	Undesirable products, lower hydrogen production
Dehydrogenation	$C_2H_5OH \leftrightarrow C_2H_4O + H_2$	Reaction pathways for hydrogen production in practice
Acetaldehyde decomposition	$C_2H_4O \leftrightarrow CH_4 + CO$	
Acetaldehyde steam reforming	$C_2H_4O + H_2O \leftrightarrow 3H_2 + 2CO$	
Dehydration	$C_2H_5OH \leftrightarrow C_2H_4 + H_2O$	Undesired pathway, main source of coke formation
Coke formation	$C_2H_4 \rightarrow$ polymeric deposits (coke)	
Decomposition	$C_2H_5OH \leftrightarrow CO + H_2 + CH_4$	Coke formation, low hydrogen production
	$2C_2H_5OH \leftrightarrow C_3H_6O + CO + 3H_2$	
	$C_2H_5OH \leftrightarrow 0.5CO_2 + 1.5CH_4$	
Reaction of decomposition products		
Methanation	$CO + 3H_2 \leftrightarrow CH_4 + H_2O$	
	$CO_2 + 4H_2 \leftrightarrow CH_4 + 2H_2O$	
Methane decomposition	$CH_4 \rightarrow 2H_2 + C$	
Boudouard reaction	$2CO \rightarrow CO_2 + C$	
Water–gas shift	$CO + H_2O \leftrightarrow CO_2 + H_2$	Reduce coke formation, enhance hydrogen production

2.1.2. Structured Catalysts, Process Intensification, and Integration

In view of the economic sustainability of ethanol reforming technologies, process intensification (PI) appears to be a pivotal step. As described above, the selection of highly active and stable catalysts is one of the possible available routes towards an economically feasible and intensified process. On the other hand, process intensification can also be achieved by reducing the external energy requirements (for example, by lowering the operating temperature), minimizing the equipment size or the feedstock costs.

The substitution of conventional fixed-bed reactors with innovative configurations characterized by high heat transfer rates and reduced mass transfer limitations is a promising strategy for developing a process intensification route, which allows reducing the reactor dimensions as well as the external heat supply [46]. Belzunge et al. [47] investigated the performance of a Pd-based catalyst in a plate microreactor (where the metallic plates present channels suitably coated with the catalyst) and demonstrated that, when the flue gas stream is recirculated in consecutive steps through the reactor, it is possible to achieve better thermal homogeneity, with a clear improvement in terms of the hydrogen production rate. The use of structured catalysts has also been investigated from a process intensification view: employing metallic monoliths or ceramic foams as the catalyst carrier can help decrease the pressure drops and enhance gas/solid transfer phenomena due to their high porosity with tortuous paths, high surface-to-volume ratios, and appropriate thermal conductivity. A Co–CeO$_2$ catalyst deposited on a FeCrAlloy monolith coated with a MgAl$_2$O$_4$ spinel layer was tested for ethanol reforming and compared with a powder sample prepared by co-impregnating Co and CeO$_2$ on a MgAl$_2$O$_4$ support [48]. In stability tests performed at 650 °C, 1 atm, and H$_2$O/C$_2$H$_5$OH = 4.9, the coated monolith was found to be more active in comparison with the packed-bed reactor, which was attributed to a lower pressure drop and a decrease in heat transfer limitations; moreover, the carbon formation rate was reduced by almost one-half in the presence of the structured carrier. Similarly, Cifuentes et al. [21] demonstrated that the performance of a Rh–Pt/CeO$_2$–SiO$_2$

powder catalyst can be enhanced by supporting it on a monolith: the reduced pressure drops recorded when using the structured catalyst led to an improvement in terms of ethanol conversion, especially between 400 and 650 °C. Moreover, the washcoated monolith was tested both in the presence of synthetic ethanol and with a glucose bioethanol feed at 700 °C, 1 atm, and $H_2O/C_2H_5OH = 3$. As depicted in Figure 4, in the presence of the raw feed, the catalyst resulted in a quite stable performance for 50 h, with a H_2/CO ratio close to that measured when using the synthetic feed. Moreover, the carbon formation rate measured in the two cases was almost the same (5.4 $mg_{coke} \cdot g_{catlyst}^{-1} \cdot h^{-1}$), demonstrating that the switch to less expensive and more sustainable sources is feasible.

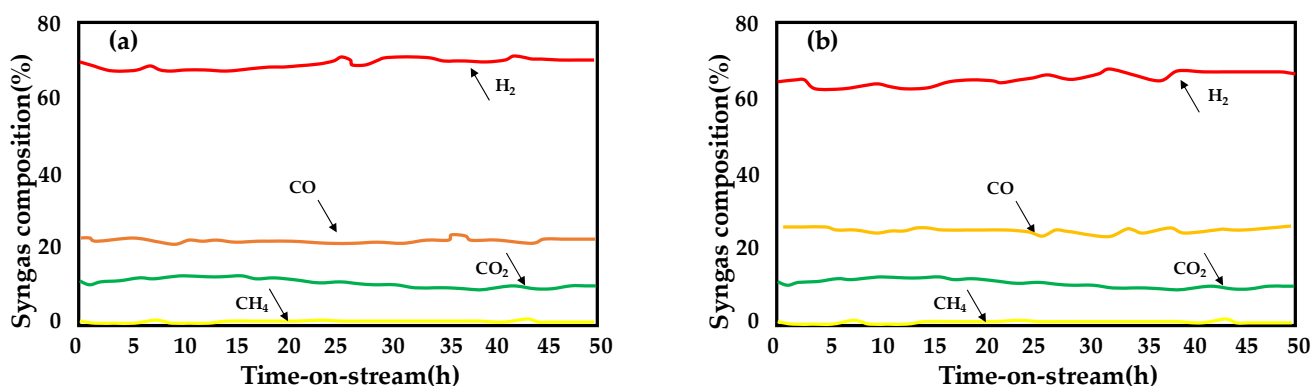**Figure 4.** Syngas composition obtained over a monolith washcoated with Rh–Pt/CeO$_2$–SiO$_2$ using (**a**) synthetic bioethanol and (**b**) actual bioethanol obtained from glucose standards. Adapted from [21]; T = 700 °C; P = 1 atm; $H_2O/C_2H_5OH = 3$; SV = 0.17 $g_{ethanol} \cdot g_{cat}^{-1}$ min^{-1}.

In fact, another strong advantage in terms of process intensification is realized by using diluted raw bioethanol solutions, characterized by much lower production costs in comparison with pure feeds. In this regard, Palma et al. [49] carried out oxidative steam reforming of ethanol over a Pt–Ni/CeO$_2$–SiO$_2$ catalyst in the presence of commercial fuel-grade bioethanol; during stability tests performed at 500 °C, P = 1 atm, and $H_2O/C_2H_5OH = 4$ for 100 h, complete ethanol conversion and H_2 yields as high as 50% were recorded, while the carbon formation rate was of the same order of magnitude as the values recorded with pure water–ethanol feeds.

Another interesting alternative for the intensification of the bioethanol reforming process is the integration of the chemical reaction with other types of unit operations in a single unit (i.e., integration of reactor and separation steps through a H_2-permselective membrane). For example, ethanol steam reforming was recently investigated at 600 °C, P = 13 atm, and $H_2O/C_2H_5OH = 6$ over an Ir/CeO$_2$ catalyst in the presence of Pd and PdCu membranes prepared by a multi-layer electroless plating method and deposited on porous ceramic tubes [50]. In both cases, the hydrogen yield and the recovery factor remained stable for 10 days of continuous operation. However, the purity of the permeated H_2 was reduced from 97% to 91% in the Cu-free membrane reformer, while a stable value of 98% was recorded when using the PdCu membrane, demonstrating that copper addition prevents leaking phenomena. Eremeev et al. [51] studied the performance of a catalytic reactor provided with a membrane made of a thin Ni–Cu alloy–Nd tungstate nanocomposite dense permselective layer deposited on a Ni–Al hierarchically structured asymmetric foam substrate. The catalyst (Ni + Ru/Pr$_{0.35}$Ce$_{0.35}$Zr$_{0.35}$O) was tested in a packed-bed configuration as well as after deposition on a honeycomb Fechralloy substrate. The influence of introducing a structured catalyst instead of the packed bed in the membrane reactor is depicted in Figure 5 as a function of the reaction temperature. When the monolith was selected, better performance was measured in terms of both H_2 yield and recovery due to the very high and stable catalytic activity recorded between 700 and 900 °C.
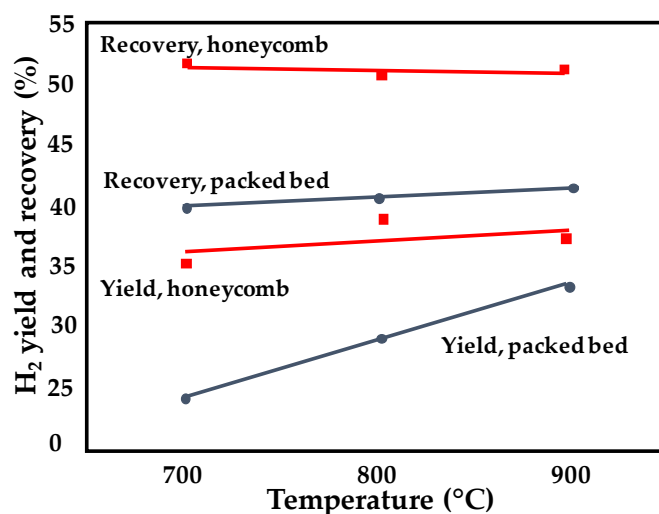
Figure 5. Change in the efficiency of a Ni–Cu membrane as a function of reaction temperature and catalytic system employed (powder vs. structured sample). Reprinted from [51]; P = 10 atm; H_2O/C_2H_5OH = 4; flow rates of 5 Nl h^{-1} for the feed gas and 10 Nl h^{-1} for the sweep gas.

Figure 6 summarizes the recent approaches implemented in the context of the ER intensification process. Due to the reaction endothermicity, the use of systems with enhanced heat transfer appears to be a promising alternative; moreover, the increase in mass transfer coefficients (obtained by microreactors of structured catalytic carriers) was shown to significantly improve catalyst activity and stability. The use of raw feeds instead of a pure water/ethanol mixture, highly desired to decrease the feedstock pre-treatment costs, was found to have a minor impact on the performance of CO_2–SiO_2-based catalysts [21,49]. Finally, the utilization of a H_2-permselective membrane combined with structured catalysts was identified as a viable route towards feasible hydrogen production from ethanol [51].
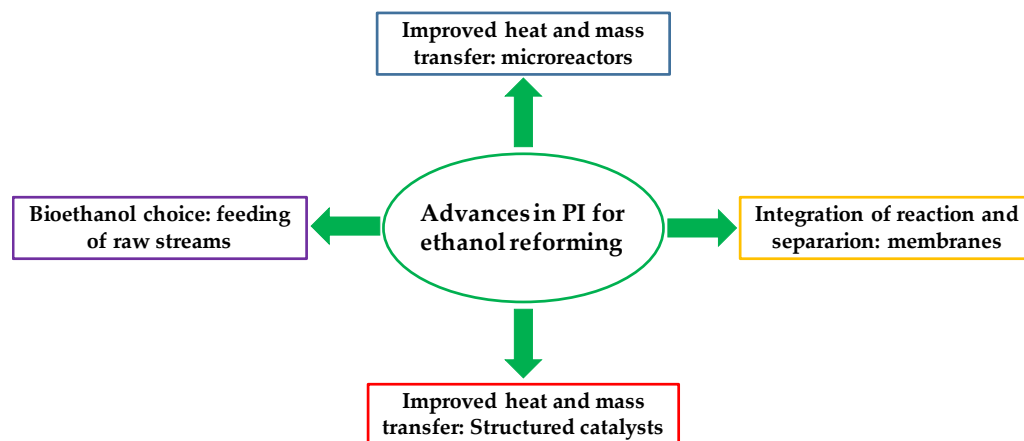

Figure 6. Main strategies followed in the last year for the intensification of ethanol reforming process.

2.1.3. Remarks

In summary, this section focuses on the main issues related to the intensification of the ethanol reforming process. Different recent strategies have been devoted to the improvement of the catalyst performance (with particular attention paid to deactivation resistance) through the investigation of various parameters (i.e., the metal loading, the preparation method, the addition of promoters, and the types of active species and supports), which may affect the active phase dispersion as well as the metal–support interaction. Other alternatives proposed to enhance industrial interest in the above process are related to the use of structured catalysts, raw bioethanol feeds, and integrated membrane reformers.

From the above discussion, it is clear that many steps forward have been taken in the last years in the framework of ethanol reforming. However, the issue of catalyst stability (which has always been the focus of industry) remains a very hot topic, and although recent strategies have been put forward to improve active metal dispersion, the actual carbon formation rates still lead to pronounced catalyst deactivation. In this regard, the use of structured catalysts and the utilization of membrane reactors may provide an interesting way to assure improved durability and high H_2 production rates. Moreover, from an operational point of view, the most advanced industrial demonstration of membrane reforming technology (which uses natural gas as the H_2 source) exploits the application of a vacuum on the permeate side to drive the reaction towards completion and increase H_2 yield (more convenient than the use of sweep gas, especially for on-site H_2 production); this strategy could also be favorable in the case of ethanol reforming [50]. Another key issue in achieving the industrial development of ethanol reforming is represented by the necessity of using inexpensive catalysts: in that respect, it is interesting to highlight that the main catalysts proposed in the last years for the above reaction (Table 1) are noble metal-free: moreover, a boost in the bioethanol production industry is also highly desired [52]. From an industrial point of view, there is also increasing interest in reducing operating temperatures for ethanol reforming, thus limiting both fixed and operating costs [53]. Finally, in view of operating with membrane reactors and considering that, in many cases, pressure swing adsorption is adopted to further purify the produced hydrogen, the study of ethanol reforming by operating at high pressures is of industrial relevance and has not been significantly investigated in the recent literature [54].

2.2. Process Intensification of WGS

WGS is an exothermic equilibrium reaction (1) and is thus thermodynamically favored at high temperatures [55], where reaction rates decline.

$$CO + H_2O \leftrightarrows CO_2 + H_2 \qquad \Delta H^\circ_{298K} = -41.4 \text{ kJ/mol} \qquad (1)$$

The heterogeneous catalytic WGS reaction plays a crucial role in hydrogen production in reforming processes, as it can be considered the first purification step of the syngas stream. Unfortunately, processes based on exothermic equilibrium reactions suffer from both thermodynamic and kinetic limitations, which are usually overcome by designing a multi-step process, in which the reaction is first carried out at a high temperature to achieve a high reaction rate at the expense of the conversion; then, after an intermediate cooling step, a further step is carried out at a low temperature to achieve high conversions at reduced reaction rates. The number of steps depends on the reaction and the aim of conversion; in the case of the water–gas shift, two adiabatic steps are conventionally carried out, HTS and LTS, in the presence of Fe/Cr-based and Cu/Zn-based catalysts under temperature regimes of 350–500 °C and 150–250 °C, respectively [56]. This configuration is effective but not efficient; the two steps are carried out in two separate reactors with two different catalytic systems, and an intercooling step is necessary; it is therefore clear that a system of this type cannot be considered optimized in terms of both size and heat management. Moreover, the hydrogen recovered at the outlet of the LTS step still contains too high a quantity of carbon monoxide; therefore, a further purification step, including methanation and preferential oxidation, must be carried out to reach 10 ppm or less for fuel cell applications (ISO 14687:2019) or 0.2 ppm or less for road vehicles and stationary appliances [57]. To optimize the WGS process, research is moving in new directions with the development of more active, stable, and eco-friendly catalysts than conventionally used ones by developing suitable catalysts for a single-stage process design and then integrating them with hydrogen- or CO_2-selective membranes. In this section, selected articles on the latest research in WGS reaction improvement and process intensification are reviewed; moreover, a summary table with the catalysts used in each reviewed article, reporting the reaction conditions and CO conversion (X_{CO}), is provided (Table 3).

2.2.1. Catalytic Formulations

The Cu/Zn-based catalysts for the LTS stage are pyrophoric, not active at temperatures higher than 350 °C, and sulfur, halogen, and unsaturated hydrocarbon intolerant [58]. On the other hand, the Fe/Cr-based catalysts for the HTS stage are not active at temperatures lower than 350 °C and suffer from over-reduction [59], and the waste may contain Cr(VI). Considerable efforts have been made to optimize the two WGS steps by studying the evolution of the active sites of conventionally used catalysts under reaction conditions and developing new formulations.

Experimental and theoretical calculations have shown that ZnO–Cu catalysts undergo Cu restructuring in situ during the WGS reaction, forming the active sites of a $Cu_{Cu(100)}$-hydroxylated ZnO ensemble [60]. The structural evolution of model Cu/ZnO catalysts during the LTS reaction was also studied through in situ transmission electron microscopy, demonstrating the dynamic nature of the atomic structures of Cu/ZnO catalysts [61]. The study showed that upon CO exposure, the Cu nanoparticles decompose and redistribute on the ZnO surface; the Cu species wet the ZnO surface to give either a defected CuOx phase or crystalline Cu_2O (Figure 7), and ZnO clusters precipitate on Cu nanoparticles and cover the Cu surface with a defected ZnOx phase. Moreover, a mixed phase of CuOx–ZnOx with an empty shell structure is present.
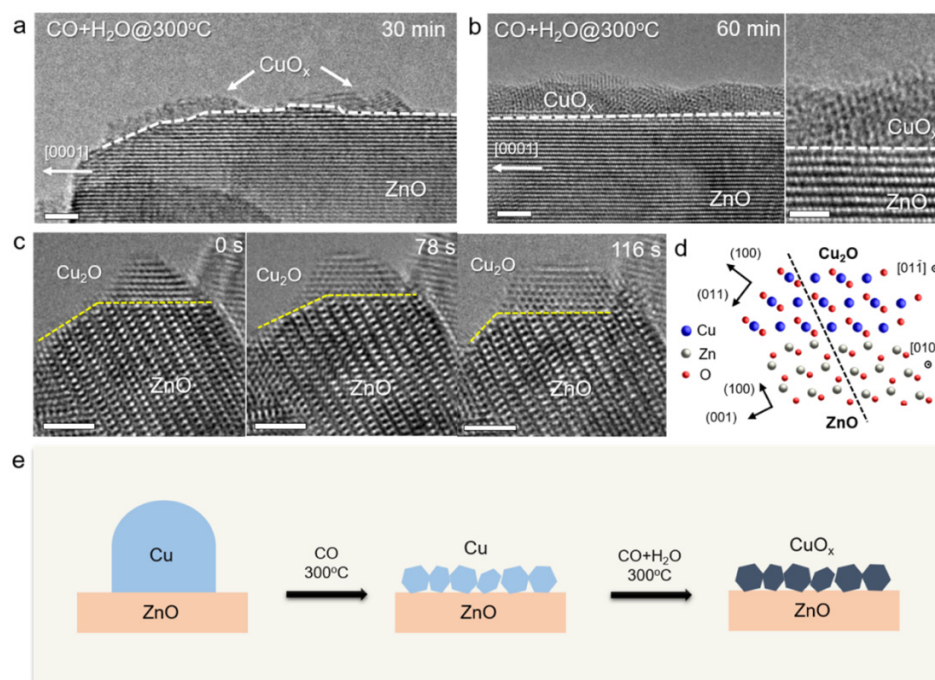

Figure 7. Wetting and reforming of Cu species on ZnO under a CO + H_2O gas mixture. (**a**) HRTEM image of the ZnO surface wet with disordered CuOx nanoislands after a 30 min exposure to the CO + H_2O (1:1) gas mixture. (**b**) HRTEM image shows an overlayer of CuOx species on ZnO with a thickness of ~2 nm after a 60 min exposure to the same gas mixture. (**c**) A series of time-resolved HRTEM images depicts the growth process of the Cu_2O nanoparticle on a terrace of the ZnO surface. (**d**) Atomic model of Cu_2O and ZnO forming an intimate interface at the atomic scale. (**e**) Schematic shows the structural evolution of Cu/ZnO under CO and CO + H_2O treatment. All scale bars are 2 nm. Adapted from [61].

Preparation methods and changes to the catalytic formulation have been studied to obtain controlled-size active phases. Cu/SiO_2 derived from copper phyllosilicate prepared via an ammonia evaporation method showed higher activity and stability in LTS than a catalyst with the same chemical composition prepared via the conventional impregnation method [62]. The presence of stable Cu^+ sites is promoted by the unique structural features of phyllosilicate; moreover, copper nanoparticles with diameters of around 3 nm are

uniformly distributed on the silica support. Particularly interesting is the metal/reducible support catalytic system; these kinds of catalysts are usually described as bifunctional systems with an active metal and reducible support, such as ceria, which governs different steps of the reaction mechanism. DFT and microkinetic calculations for WGS on the CeO_2(111) surface have suggested a combination of redox and associative mechanisms as the main reaction pathway at low temperatures [63]. This mechanism suggests an active role of oxygen vacancies on the ceria surface, which has intrinsic activity and can also facilitate the release of hydrogen when supporting an active metal by preventing the blocking of active sites by hydroxyl groups. When precipitating ceria from a cerium nitrate solution, the K_2CO_3/KOH ratio is crucial in determining the physicochemical properties of Cu/CeO_2 catalysts. An increase in the K_2CO_3/KOH ratio improves the oxygen storage capacity but decreases Cu dispersion, thus suggesting that the optimum ratio value is around 3 [64]. The Cu/CeO_2 catalytic system shows an activity of one order of magnitude higher than other copper-based catalysts, which is attributed to the presence of oxidized Cu species, even when in a reductive atmosphere, thanks to the O diffusion of CeO_2 from the bulk to the surface [65]. Theoretical studies have demonstrated that the activity of Cu/CeO_2 catalysts in the LTS reaction is related to the shape of the ceria support (particles, rods, and cubes) [66]. The density of the defect sites of ceria determines the geometrical structure and the chemical state of copper species, suggesting that the active sites can be tuned by dispersing Cu species on shape-controlled ceria particles.

An α-MoC-based catalyst modified by Ir1 single atoms showed a CO conversion of ~100% at 150 °C and a specific reaction rate that was 2 orders of magnitude higher than that of FeOx- or Al_2O_3-supported Ir1 catalysts [67] and ~4 times that of α-MoC [68]. The results of the study suggest that iridium is not directly involved in the catalysis; rather, it can be considered a promoter that affects the electronic structure of active Mo sites.

In the case of HTS catalysts, attention has been focused on the role of chromium in the reaction mechanisms, with the aim of suggesting sustainable alternatives. Experimental investigations have shown that chromium-doped magnetite can be formed after exposing the calcined catalyst to industrially relevant HTS conditions [69]. Mössbauer spectra have shown the incorporation of chromium in the octahedral sites of magnetite, which prevents the reduction of Fe^{3+} ions and increases the Fe^{3+}/Fe^{2+} ratio in octahedral sites. DFT calculations show that chromium is preferentially located below FeO_6 sites; moreover, chromium replacement in the structure increases the vacancy formation energy but does not affect the location, thus confirming that chromium cannot be considered a chemical promoter [70]. Chromium can be considered a structural promoter since, by replacing some Fe^{3+}, it deforms the reticence of magnetite, increasing the surface area and the intrinsic catalytic activity of iron oxide crystallites [71]. The CuCrFeOx catalyst has also been studied, and the results demonstrate that it is partially reduced under reaction conditions with metallic Cu nanoparticles on the Fe_3O_4 surface; moreover, DFT calculations found the redox mechanism to be energetically favored over the associative mechanism [72]. Mössbauer spectra demonstrate that copper doping does not affect the magnetite structure; the copper is in a separate phase, in the metallic state, as shown by near-ambient pressure XPS [73]. Doping with cerium or co-doping with cobalt or chromium increases the stability of the magnetite phase, preventing sintering and suppressing coke formation due to a decrease in the Fe^{3+}/Fe^{2+} ratio on the surface of ternary spinel ferrites [74].

Alternative catalytic systems for high temperatures have been proposed, such as perovskite-type oxides, the great compositional flexibility of which allows the rational design of the catalyst. In fact, both cation sites (A and B in ABO_3) can be doped with promoters or catalytically active elements, and the exsolution of B-site dopants can strongly boost catalytic performance [75]. Comparative studies in which the composition of A and B sites was doped with various metals have shown that Ni and Co provide the highest activity [75]. Ni-based catalysts supported on SBA-15 with incorporated Zr and/or Ce were studied to evaluate the effect of zirconium and cerium ions in the silica framework in the HTS reaction [76]. The presence of Zr and Ce in the silica framework can minimize

the formation of Ni subcarbonyl species and enhance the adsorption of CO on Ni. The best catalytic activity was obtained with Ni/Zr–Ce-SBA-15; the turnover frequency was $4.57 \, s^{-1}$, and the hydrogen formation rate was 534 μmol $H_2 \, g^{-1} s^{-1}$. The use of nickel as an active component in the HTS reaction is extremely attractive due to the low cost; however, its propensity to catalyze methane formation represents a major limitation to its use. The results of a recent comparative study on Ni–Cu/CeO_2–Al_2O_3 catalysts demonstrate that the addition of Cu has an important role in suppressing methane production via the creation of the Ni–Cu alloy [77]. On the other hand, the addition of sodium to catalysts based on nickel supported on anatase shows higher catalytic activity than that of their counterparts supported on rutile and a mixture of rutile and anatase [78]. It has also been demonstrated that a layer of titanate that forms on the surface promotes the reduction of the support and suppresses the encapsulation of nickel in the support. Consequently, a higher number of oxygen vacancies and better exposure of the metal surface generate higher catalytic activity in the WGS reaction. Furthermore, methanation is suppressed thanks to the weak adsorption of H_2 on suitable species on the catalyst. The density of oxygen vacancies is related to the extent of alkali doping in the titanate overlayer formed in situ via alkali doping [79]. Sodium-doped Ni/TiO_2 with a titanate overlayer on the support shows higher activity in the WGS reaction compared to the undoped catalyst.

As an alternative to conventional catalysts, noble metals based on highly reducible rare-earth oxide-based catalytic formulations have proven to be usable in a wide temperature range, not only for LTS but also for intermediate temperatures. Among noble metal-based catalysts, those based on gold or platinum are the most studied; the former is highly active at lower temperatures, while the latter shows higher stability.

Au-based catalysts are commonly activated through a calcination step to construct an active Au/support interface, which unfortunately causes the sintering of Au nanoparticles [80]. As an alternative, O_2 plasma enables the control of the Au nanoparticle size and the creation and modulation of the electronic structure of Au/TiO_2 interfaces, thus improving H_2O activation and dissociation, which affect the WGS reaction rate [80]. The performance of mixed ceria/praseodymium-supported Au clusters was studied by varying the Ce/Pr ratio (4:1, 2:1, and 1:4), showing that the catalyst with a ratio equal to 4/1 exhibited the highest activity, about 5 times that of Au/CeOx [81]. This result was attributed to the lowest oxygen vacancy formation energy and the highest H_2O binding energy in the presence of Au/$Ce_4Pr_1O_x$. Double-layered supports are particularly attractive for catalytic applications; in particular, gold nanoparticles supported on ZnCr layered double hydroxides showed the best performance in the WGS reaction in a comparative study among different layered double hydroxides (ZnM-; M = Al, Cr, or Fe) [82]. The results were related to the lower activation energy. Similarly, gold-based catalysts supported on co-precipitated NiAl and NiMgAl layered double hydroxides showed good activity in the WGS reaction [83]. The performance was attributed to the dual role of magnesium, which contributes to improving the Ni^{2+} ion dispersion and reducing the surface acidity of Ni–Mg–Al metal oxide formed during the reaction at high temperatures. Moreover, the addition of ceria to gold supported on nanosized NiAl layered double hydroxides showed improved performance in the WGS reaction because it resulted in the highest dispersion of gold particles [84]. CeO_2–ZnO porous nanorods have been used to control the size and to prevent the sintering of Au nanoparticles; moreover, the presence of zinc oxide prevents the formation of undesired side products such as CH_4 and CH_3OH [85].

Ceria supports have been extensively used in the preparation of platinum-based catalysts, demonstrating that the synthesis procedure plays a crucial role in determining the Pt dispersion and metal–support interaction, which depends on the morphology of the support. The urea-assisted homogeneous precipitation method improves the redox and electronic abilities of the support, leading to better performance of the resulting Pt/CeO_2 catalysts compared to corresponding catalysts in which the support is obtained by microwave-assisted hydrothermal synthesis and polymer-assisted hydrothermal synthesis [86]. The reaction mechanism of a platinum-based catalyst supported on ceria was also

studied, showing that, under working conditions, the reaction proceeds via the redox path at the dynamic perimeter Pt^0-O vacancy-Ce^{3+} site, where CO oxidation, water reduction, and hydrogen recombination occur [87]. Enhanced activity was obtained by alloying Pt with iron [88]; TG and XRD analysis showed that the alloy does not undergo oxidation under reaction conditions until 350 °C. The introduction of a second metal was also studied; among Fe, Co, and Ni, the best performance was observed with iron, attributed to the adjustment of the electronic structure of platinum to a moderate oxidation state [89].

Table 3. Selected catalysts in reviewed articles in WGS section: reaction conditions and CO conversion (X_{CO}).

Selected Catalyst	Reaction Conditions	CO Conversion; Time on Stream	Reference
9%ZnO/c-Cu-34	$CO/H_2O/Ar = 5/10/85$; 200 °C; GHSV = 3600 h^{-1}	$X_{CO} \approx 80\%$	[60]
Cu/SiO$_2$	$CO/H_2O/He = 5/5/40$; 250 °C; GHSV = 30,000 h^{-1}	$X_{CO} \approx 27\%$; 24 h	[62]
Cu/CeO$_2$	$CO/CO_2/CH_4/H_2/H_2O/N_2 = 9/10/1/60/60/20$; 360 °C; GHSV = 50,102 h^{-1}	$X_{CO} \approx 60\%$; 110 h	[64]
20CuCe-NS	$CO/H_2O/N_2 = 2/10/88$; 250 °C; GHSV = 42,000 h^{-1}	$X_{CO} \approx 92\%$; 73 h	[65]
Cu/CeO$_2$	$CO/H_2O/N_2 = 1/3/96$; 200 °C; GHSV = 40,000 h^{-1}	$X_{CO} \approx 30\%$; 12 h	[66]
Ir/α-MoC	$CO/H_2O/He = 2/10/88$; 150 °C; GHSV = 18,000 h^{-1}	$X_{CO} \approx 100\%$	[68]
Cr$_2$O$_3$α-Fe$_2$O$_3$	$H_2/CO/CO_2/N_2/H_2O = 37/9/4/17/33$; 450 °C	$X_{CO} \approx 75\%$; 90 h	[69]
α-Fe$_2$O$_3$/Cr$_2$O$_3$/CuO	$H_2/CO/CO_2/N_2/H_2O = 37/9/4/17/33$; 450 °C; 25 bar	$X_{CO} \approx 75\%$; 90 h	[73]
FeCeCoOx Ni/Zr–Ce-SBA-15	$CO/H_2O = 2/7$; 500 °C; 20 bar; GHSV = 30,000 h^{-1} $CO/H_2O/He = 5/25/70$; 400 °C; GHSV = 40,000 h^{-1}	$X_{CO} \approx 90\%$; 150 h $X_{CO} \approx 98\%$; 70 h	[74] [76]
7Ni-7.5Cu/CeO$_2$–Al$_2$O$_3$	$H_2/CO/CO_2/H_2O = 6/3/1/6$; 400 °C; GHSV = 30,000 h^{-1}	$X_{CO} \approx 35\%$; 20 h	[77]
Ni/TiO$_2$(A)-Na	$CO/H_2O/He = 5/20/75$; 350 °C, GHSV = 60,000 mL·g^{-1}·h^{-1}	$X_{CO} \approx 42\%$; 8 h	[78]
Ni–Na-R350	$CO/H_2O/He = 5/20/75$; 350 °C; GHSV = 20,000 mL·g^{-1}·h^{-1}	$X_{CO} \approx 98\%$	[79]
Au/TiO$_2$	$CO/H2O/He = 5/10/85$; 150 °C; GHSV = 12,000 mL·g^{-1}·h^{-1}	$X_{CO} \approx 70\%$; 4 h	[80]
Au/Ce$_4$Pr$_1$O$_X$	$CO/H_2O/N_2 = 2/10/88$; 300 °C; GHSV = 54,000 mL·g^{-1}·h^{-1}	$X_{CO} \approx 70\%$; 50 h	[81]
Au/ZnCr-LDHs	$CO/H_2O/Ar = 3/15/82$; 300 °C; GHSV = 90,000 mL·g^{-1}·h^{-1}	$X_{CO} \approx 75\%$; 50 h	[82]
Au/NiMgAl	$CO/H_2O/Ar = 3.76/25.01/71.23$; 260 °C; GHSV = 4000 h^{-1}	$X_{CO} \approx 95\%$	[83]
Au/eCeNiAl	$CO/H_2O/Ar = 3.76/25.01/71.23$; 220 °C; GHSV = 4000 h^{-1}	$X_{CO} \approx 99\%$	[84]
Pt/CeO$_2$-urea	$CO/H_2O/H_2/CO_2/He = 7/30/50/9/4$; 380 °C; GHSV = 40,000 mL·g^{-1}·h^{-1}	$X_{CO} \approx 70\%$	[86]
Pt$_{0.5}$Fe$_{0.5}$/SiO$_2$	$CO/CO_2/H_2O/H_2 = 10/15/30/45$; 350 °C; GHSV = 75,000 mL·g^{-1}·h^{-1}	$X_{CO} \approx 55\%$	[88]
PtRe/CeO$_2$/Al-foam	$H_2/CO_2/CO/H_2O/CH_4 = 37.41/9.31/9.31/42.19/1.37$; 330 °C; τ = 53 ms	$X_{CO} \approx 85\%$	[90]
1Pt/1Re/CeZrO$_4$/Al$_2$O$_3$/Al-foam10_10	$CO/CO_2/H_2O/H_2/N_2 = 5.36/5.36/26.56/42.72/20$; 300 °C; GHSV = 20,000 h^{-1}	$X_{CO} \approx 90\%$	[91]
PtCeAl-ZrEuMo/monolith	$CO/CO_2/H_2O/H_2 = 9/11/30/50$; 330 °C; GHSV = 80,000 mL·g^{-1}·h^{-1}	$X_{CO} \approx 25\%$; 70 h	[92]
Pt/CeO$_2$/Al-monolith	$CO/H_2O/N_2 = 8/30/62$; 255 °C; τc = 360 ms	$X_{CO} \approx 99\%$	[93]
Pt/CeO$_2$/Al-sponge	$CO/H_2O/N_2 = 8/30/62$; 320 °C; τc = 38 ms	$X_{CO} \approx 55\%$; 35 h	[94]

2.2.2. Structured Catalysts, Process Intensification, and Integration

The idea behind the design of the single-stage WGS process primarily focuses on the assumption that a small plant and a smart process must be used for the distributed production of hydrogen, i.e., the on-site production of hydrogen. The best candidates to realize this kind of reactor configuration seem to be structured catalysts, obtained

by coupling conductive structure and catalytic formulations active in both the LTS and in HTS temperature ranges. Recent studies have demonstrated that a good scale-up of the catalytic performance from the powder to the structured catalyst can be achieved, thus obtaining comparable performance to catalytic formulations based on noble metals such as platinum supported on reducible oxides such as ceria loaded on aluminum foam monoliths [90]. The presence of the conductive structure allows reducing the temperature difference between the inlet and the outlet of the catalytic bed due to the heat generated under reaction conditions. The temperature at the inlet of the catalytic bed increases while the temperature at the outlet decreases compared to the case of the powder catalyst as a result of the back diffusion of heat on the conductive structure, thus obtaining a beneficial effect on both the kinetics and CO conversion [91]. The kinetics of the WGS reaction was studied on a Pt-based washcoated microchannel metal structure [92], showing that the rate expression is independent of the CO concentration, the inhibiting effect of hydrogen, and the promoting effect of water. The reaction order was around zero for carbon monoxide, negative for hydrogen, and 0.36 for water, which is significantly lower than that reported for non-promoted catalysts (typically 0.77–1.10) due to the water-enhancing effect of the proton conductor in the rate-limiting step. The shape of the structure can play a crucial role in determining the performance of the catalyst; a comparative study between aluminum honeycomb monolith and foam, washcoated with the same catalytic formulation, highlighted that the best performance was obtained by the foam-structured catalyst [93]. The study revealed a high resistance to heat exchange at the solid–gas phase interface of the honeycomb monolith system due to the flow field developed in the channels. The tortuosity of the foam system favored the axial and radial heat and mass transfer, giving rise to a more homogeneous distribution, higher temperatures, faster kinetics, and higher carbon monoxide conversion. It has been demonstrated that a narrow distribution of porosities can prevent the formation of preferential directions in foam-structured catalysts. Moreover, the presence of "bottleneck"-type connections among the pores is beneficial in catalytic systems [94].

A promising alternative to conventional fixed-bed reactors is a membrane reactor in which hydrogen and/or carbon dioxide can be removed through the membrane during the reaction, thus increasing the conversion beyond the equilibrium until the limitations imposed by reaction kinetics become dominant [95]. The enhanced WGS reaction was performed in an integrated Pd–Cu catalytic membrane reactor at a high temperature, obtaining an increase in the conversion rate of 10.0–16.7% and an increase in CO conversion from 85.4% to 94.8% compared to the fixed-bed catalytic reactor [57] Simulation studies have demonstrated that a single-stage HTS ceramic−carbonate dual-phase membrane reactor is able to provide high-purity CO_2 with a capture ratio over 98%, while the high-pressure hydrogen in the retentate has a purity higher than 90% [57].

2.2.3. Remarks

In this section, an overview of the latest research in the WGS process is provided. Table 4 summarizes the objects of the studies of the reviewed articles with their main findings. The interest of researchers has been focused on alternatives to conventional catalysts for HTS and LTS; Ni-based catalysts have shown good performance at high temperatures, while the use of α-MoC modified by a Ir1 single-atom catalyst is attractive at low temperatures. The stability of Au-based catalysts has been addressed, and the use of O_2 plasma and double-layered supports can overcome the main obstacles to their use. Conductive structured catalysts and integration into membrane reactors are the basis for designing a single-stage process, which is the most viable route to obtain high-purity hydrogen.

The results of these studies are extremely significant and allow us to propose a way to realize the strong intensification of the process. The demand for energy and the growing need to reduce process production costs have decisively conditioned the direction taken in research on new catalysts and new reactor configurations. The global WGS process,

conceived in two steps, seems to be inadequate for meeting the need for efficient production processes, which should use renewable energy sources, which are inevitably linked to the resources of the individual territories. On-site production requires a reduction in the size of the plants, especially in the case of hydrogen, which is considered the most powerful energy vector. In this context, the single-stage WGS process seems to be the only viable path. An efficient single-stage WGS process completely converts carbon monoxide without depressing the kinetics; therefore, it must be designed at medium-high temperatures and possibly integrated with an efficient purification system, for example, a membrane. To achieve this, modifications to conventional catalysts for LTS and HTS have been made in recent years to make them active in a wider temperature range; as an alternative, structured conductive catalysts have been developed, which have the advantage of managing the reaction heat in an innovative way compared to traditional pellets. In all cases, from the data reported in the literature, the use of reducible oxides seems to be essential to obtaining more active and stable catalysts. Furthermore, integration with membranes requires further studies to be considered feasible.

Table 4. Schematic summary of the main findings resulting from the reviewed articles of the WGS section.

Object of the Study	Main Findings	Ref.
The structure of LTS catalysts	ZnO–Cu catalysts undergo in situ Cu restructuring during the WGS reaction, forming a mixed phase of CuOx–ZnOx with an empty shell structure.	[60,61]
Alternative LTS catalytic systems	Cu-based catalysts supported on various oxides (SiO_2, CeO_2) are proposed. α-MoC modified by Ir1 single-atom catalyst shows a CO conversion of ~100% at 150 °C. Ir is a promoter that affects the electronic structure of active Mo sites.	[62,68]
The role of chromium in HTS catalysts	Chromium is a structural promoter, and its incorporation in the octahedral sites of magnetite prevents the reduction of Fe^{3+} ions. Doping with a metal may affect the Fe^{3+}/Fe^{2+} ratio on the ferrite surface.	[69–74]
Alternative HTS catalytic systems	Ni-based catalysts are the most interesting alternative to conventional HTS catalysts. These include both perovskite-type oxides and those supported on various oxides such as SBA, ZrO_2, CeO_2, and TiO_2.	[75–79]
Au-based catalyst activation and stability	O_2 plasma allows control of the Au nanoparticle size and modulation of the electronic structure at interfaces. Double-layered support and nanorods allow better dispersion of Au nanoparticles.	[80–85]
Pt-based catalyst activity	The metal–support interaction depends on the morphology of the support. The redox path at the dynamic perimeter Pt^0-O vacancy-Ce^{3+} site is preferred. The bimetallic PtFe system shows enhanced activity both as alloy and when supported on ceria.	[86–89]
Comparison between powder and conductive structured catalysts	The improved management of the reaction heat on the conductive structured catalyst is beneficial for kinetics and CO conversion.	[90,91]
Pt-based washcoated microchannel metal structure	The reaction order is around zero for carbon monoxide, negative for hydrogen, and 0.36 for water.	[92]
Structured catalyst reactor configuration	Foam structures provide improved heat and mass transfer compared to the honeycomb monolith structure.	[93,94]
Ceramic–carbonate dual-phase membrane reactor	Hydrogen purity > 90%, CO_2 capture ratio > 98%.	[95]
Integrated Pd–Cu membrane reactor	The conversion rate increases by 10.0–16.7%, and Co conversion increases from 85.4 to 94.8%.	[57]

2.3. CO₂ Catalytic Hydrogenation to Hydrocarbons

The continuously increasing CO_2 levels in the atmosphere have mandated the development of innovative strategies and technologies to reduce their emissions [96] Currently, the use of CO_2 as a raw material is becoming promising in the context of sustainable development and environmental protection [97] CO_2 is already used in different fields, such as food processing, drinks, medicine, and industry, but these sequestration methods are characterized by temporary operation [98] However, CO_2 may also be used in the synthesis of fine chemicals and fuels, representing a promising approach for feedstock substitution in a sustainable way [99] In this aspect, the CCU approach allowed the development of both CO_2 capture and separation technologies, as well as efficient catalytic systems for the conversion of CO_2 [100] The latter are particularly relevant to the aim of employing waste biomass, which produces undesired carbon dioxide, as mentioned in Section 2. Indeed, without any CO_2 utilization technology coupled with biomass fermentation, there is a loss in the overall sustainability of the process.

According to the literature on catalytic CO_2 valorization, either homogeneous or heterogeneous catalysts may be used for converting it into the desired product [101] Different studies have focused on the use of various homogeneous catalysts, such as frustrated Lewis pairs, transition metal complexes, and N-heterocyclic carbenes with good activity towards CO_2 reduction [102,103]. However, this route is characterized by low process efficiency, and the separation of the catalyst from the product is very difficult. Therefore, research efforts have focused on CO_2 reduction by using heterogeneous catalysts through thermal, electrochemical, photochemical, biochemical, and plasma techniques [104], which are briefly described in the following lines. The electrocatalytic reduction of CO_2 has several advantages over other processes, since it produces less environmental damage due to mild operating conditions and easily controllable reaction rates. In addition, since the required H_2 typically comes from water, it does not need to work under high-pressure conditions as thermal reduction does. However, two main disadvantages of this technique can be considered: (i) the high cost of electricity, which must be generated from renewable sources (hydrothermal, geothermal, solar wind, etc.), and (ii) limited CO_2 conversion [105]. The photochemical reduction of CO_2 consists in the use of visible light harvested from the sun, which, in the presence of semiconducting materials (i.e., oxides, sulfides, and phosphides), is employed to generate photo-excited electrons and holes for the reduction process [104] This process is affected by low efficiency, which does not favor its industrial commercialization, even if it has the advantage of utilizing readily available solar energy [106–108]. The biochemical method offers an eco-friendly approach to producing carbon-based chemicals from CO_2 reduction. However, it is affected by the high cost of catalysts and co-factors [109] The plasma-assisted catalytic approach to CO_2 reduction is acquiring increasing research attention. The process can solve the challenges involved in CO_2 activation owing to its inertness [110] The combined use of a dielectric barrier discharge (DBD) reactor and a suitably developed catalyst operating in a non-equilibrium environment may result in improved conversion efficiency and enhanced selectivity to target value-added products, as described in the following subsection. Among all of the advantages, there is a trade-off between energy and conversion efficiency. The thermochemical process is the conventional technique in which, by using a solid catalyst and in the presence of heat energy, CO_2 can be hydrogenated into a wide variety of products (alkanes, alkanes, methanol, dimethyl ether, formic acid, etc.). For this purpose, two different approaches can be considered: using either a "standalone" catalyst (direct CO_2 hydrogenation) or a "tandem" catalyst (a catalyst composed by combining zeolites with either Fe-based Fischer–Tropsch synthesis (FTS) or metal oxide-based methanol synthesis catalyst). Different studies have demonstrated that catalytic properties and reaction conditions can be tuned to achieve various product distributions (light/heavy olefins, paraffin, aromatics, etc.). In the former approach, through the reverse water–gas shift (RWGS) reaction, the standalone catalyst converts CO_2 to CO, which is subsequently converted into hydrocarbon products via FTS in a multi-step process [109] This approach is henceforth designated as the CO_2 modified-FT

process. In the latter approach, a hydrogenation catalyst is used for converting CO_2 to CO or methanol, followed by the further transformation of methanol to hydrocarbons over a zeolite catalyst. This sequence of processes can be achieved in separate reactors or coupled in a single reactor [105] For example, olefin synthesis can be obtained through a two-step process, with the first step consisting of a CO_2-FT catalyst hydrogenating CO_2 to a wide range of hydrocarbon products (via CO intermediate) and the second one consisting of a downstream zeolite catalyst bed for product redistribution. In the integrated one-step process, a bifunctional catalyst is present, which simultaneously allows obtaining both the synthesis and dehydration reactions of methanol. CO_2 is mostly hydrogenated to methanol (via a methanol-mediated route), followed by methanol conversion to olefins (MTO) on bifunctional active sites [111,112]. Recent research activities have focused on the development of efficient and stable catalysts, among which the development of metal oxide and MFI structured zeolite composite catalysts provides a new platform for the direct production of aromatics from CO_2 [113].

The simultaneous production of methanol and olefins in a single step allows avoiding the accumulation of methanol in the reactor, thus increasing CO_2 conversion by overcoming thermodynamic equilibrium limitations. In addition, the occurrence of both reaction steps synchronously is favorable from the economic point of view, as only one reactor is required [114,115]. Several modified-FT catalysts have been reported to effectively catalyze CO_2 hydrogenation to lower olefins (CTLO), including Fe, Cu, and Co-based catalysts over appropriate metal-oxide supports [105]

2.3.1. CO_2 to HC through Methanol Pathway

CO_2 conversion into methanol has been extensively studied by the scientific community, and among different catalysts, those based on Cu/ZnO are the most widely investigated [116] However, despite the successes that have been reported, the reaction pathway is still unclear. In fact, formate species (HCOO*) and hydrocarboxyl species (COOH*) have each been reported as the first hydrogenation products. The formation of hydrocarbons from methanol is mainly achieved with the aid of a zeolitic catalyst, generally HZSM-5 and/or SAPO-34 [117] More than 20 possible mechanisms have been proposed for the reaction [105] However, the dual HC pool mechanism is of great interest. HC intermediates, specified as $(CH_2)_n$, represent the adsorbate and may also contain several poly-condensed aromatic species characterizing coke (containing less H than indicated). Recent studies have shown that the mechanism of methanol-to-HC conversion proceeds via two steps:

1. A short induction period, in which the coupling of two methanol molecules through surface methoxy species allows the direct configuration of the C–C bond [118,119];
2. An autocatalytic dual-cycle mechanism, in which different reactions occur, including the methylation and cracking of olefin, methylation and dealkylation of aromatics, H_2 transfer, and cyclization [120,121], controlling the lifetime of the catalyst and selectivity of the product.

The product distribution mainly depends on the topological structure of zeolite, its acidity, and operating conditions [122].

Very recently, tandem catalysts constituted by metal oxides and HZSM-5 zeolites with different morphologies (spherical, hollow, sheet, and chain) were studied [113]. The research demonstrated that the ZSM-5 morphology is important in determining the catalyst performance, with higher CO_2 conversion and selectivity to the desired product shown by the sheet and chain configurations, respectively. Zeolites with different topologies in combination with metal oxides have also been investigated, and the results revealed that the pore dimensions of the zeolites are fundamental for directing the products towards the desired ones [123–125]. In particular, the larger the pores are, the heavier the obtained hydrocarbons are. The results of these recent studies are summarized in Table 5.

Table 5. Innovative tandem catalysts developed for CO_2 hydrogenation through methanol pathway, tested at CO_2/H_2 feed ratio of 1:3.

Catalyst	Reaction Conditions	CO₂ Conversion	Reference
ZnZr₇O(500)-sheetZ5	360 °C; 3 MPa; 4800 mL·g⁻¹ h⁻¹	17.2%	[113]
ZnZr₇O(500)-hollowZ5	360 °C; 3 MPa; 4800 mL·g⁻¹ h⁻¹	14.1%	[113]
ZnZr₇O(500)-sphericalZ5	360 °C; 3 MPa; 4800 mL·g⁻¹ h⁻¹	10.8%	[113]
ZnZr₇O(500)-chainZ5	360 °C; 3 MPa; 4800 mL·g⁻¹ h⁻¹	13.5%	[113]
In₂O₃-sheetZ5	360 °C; 3 MPa; 4800 mL·g⁻¹ h⁻¹	24.9%	[113]
Cu–ZnO–Al₂O₃-sheetZ5	360 °C; 3 MPa; 4800 mL·g⁻¹ h⁻¹	34.5%	[113]
ZnZrOx + MOR	375 °C; 10 bar; 2100 mL·g⁻¹ h⁻¹	20.9%	[123]
ZnZrOx + SAPO-34	375 °C; 10 bar; 2100 mL·g⁻¹ h⁻¹	17.9%	[123]
ZnZrOx + ERI	375 °C; 10 bar; 2100 mL·g⁻¹ h⁻¹	23.6%	[123]
ZnZrOx + MFI	375 °C; 10 bar; 2100 mL·g⁻¹ h⁻¹	22.0%	[123]
13%ZnO–ZrO₂	380 °C; 2.0 MPa; 4800 h⁻¹; ratio of ZnO–ZrO₂ to zeolite = 1	15.9%	[124]
13%ZnO–ZrO₂/ SAPO-34	380 °C; 2.0 MPa; 4800 h⁻¹; ratio of ZnO–ZrO₂ to zeolite = 1	17.3%	[124]
13%ZnO–ZrO₂/ Mn₀.₁SAPO-34	380 °C; 2.0 MPa; 4800 h⁻¹; ratio of ZnO–ZrO₂ to zeolite = 1	21.3%	[124]
13%ZnO–ZrO₂/ Zn₀.₁SAPO-34	380 °C; 2.0 MPa; 4800 h⁻¹; ratio of ZnO–ZrO₂ to zeolite = 1	18.0%	[124]
13%ZnO–ZrO₂/ Zr₀.₁SAPO-34	380 °C; 2.0 MPa; 4800 h⁻¹; ratio of ZnO–ZrO₂ to zeolite = 1	19.6%	[124]
ZnO/SAPO-34-BM	380 °C; 3.0 MPa; 3600 mL g⁻¹ h⁻¹; ratio of oxide to zeolite = 3:1	18.1%	[125]
5%Mn₂O₃–ZnO/SAPO-34-BM	380 °C; 3.0 MPa; 3600 mL g⁻¹ h⁻¹; ratio of oxide to zeolite = 3:1	23.9%	[125]
20%Mn₂O₃–ZnO/SAPO-34-BM	380 °C; 3.0 MPa; 3600 mL g⁻¹ h⁻¹; ratio of oxide to zeolite = 3:1	29.8%	[125]
20%Mn₂O₃/ZnO/SAPO-34-BM	380 °C; 3.0 MPa; 3600 mL g⁻¹ h⁻¹; ratio of oxide to zeolite = 3:1	19.9%	[125]
70%Mn₂O₃–ZnO/SAPO-34-BM	380 °C; 3.0 MPa; 3600 mL g⁻¹ h⁻¹; ratio of oxide to zeolite = 3:1	21.6%	[125]
Mn₂O₃/SAPO-34-BM	380 °C; 3.0 MPa; 3600 mL g⁻¹ h⁻¹; ratio of oxide to zeolite = 3:1	8.8%	[125]

2.3.2. CO₂ to HC through RWGS

Among all of the available catalysts for CO_2 conversion via the RWGS process, Fe-based catalysts have attracted worldwide attention [126]. In the initial stage, CO_2 is converted into CO, which is subsequently hydrogenated to olefins and paraffin on active sites of Fe-carbide, as proposed by Xu et al. [127]. By means of a bifunctional system (such as acidic zeolite), the so-obtained olefins and paraffin products are then converted into other hydrocarbons through different reactions of aromatization, hydrocracking, hydro-isomerization, oligomerization, and cyclization plus H-transfer. The reaction chemistry is apparently very complex and therefore produces various reaction intermediates [127,128]. Monomolecular and bimolecular activation mechanisms have been proposed for paraffin conversion into HC. The former mechanism was proposed by Haag et al. [129] who described the protonation of the alkane molecule to form carbonium ions that can undergo C–C or C–H bond cleavage. Subsequently, the carbonium ions produce olefin via the back-donation of a proton to zeolite. The latter mechanism can be achieved by the protonation of paraffin using the Bronsted acid site, which is then used to form a dimer with another olefinic HC [130,131]. Once the paraffin activation is achieved, subsequent conversion into various HCs proceeds. Catalytic cracking can proceed through both bimolecular and monomolecular mechanisms. However, the monomolecular mechanism predominantly occurs at high temperatures, while the bimolecular mechanism usually occurs at a mild temperature (<350 °C). Aromatization can proceed through polymerization reactions to form dienes [132], which is then followed by cyclization in zeolite channels and multi-step H-transfer with olefin, yielding aromatics and paraffin [133]. Subsequently, inter-conversion reactions such as isomerization, disproportionation, and alkylation/dealkylation take place.

In the recent literature, Fe-based catalysts doped with either alkali metals or non-metal elements have been proposed, aiming at improving the selectivity of C_{2+} olefins [134,135]. The addition of Ce may play a key role in the activation and dissociation of adsorbed CO_2 due to the mobile oxygen vacancy in ceria oxides, which can accelerate the migration of oxygen. In this sense, FeCeNa catalysts have shown good performance in terms of CO_2 conversion to olefins [136]. The most recently proposed catalysts for HC production from CO_2 through the RWGS route are summarized in Table 6.

Table 6. Innovative catalysts for hydrocarbon production from CO_2 through RWGS route, tested at CO_2/H_2 feed ratio of 1:3.

Catalyst	Reaction Conditions	CO_2 Conversion	Reference
Fe	340 °C; 2.5 MPa; 15,000 mL g^{-1} h^{-1} GHSV	18%	[134]
Zn–Fe	340 °C; 2.5 MPa; 15,000 mL g^{-1} h^{-1} GHSV	23%	[134]
Na–Fe	340 °C; 2.5 MPa; 15,000 mL g^{-1} h^{-1} GHSV	31%	[134]
Na–Zn–Fe	340 °C; 2.5 MPa; 15,000 mL g^{-1} h^{-1} GHSV	39%	[134]
Na–Zn–Fe	340 °C; 2.5 MPa; 300,000 mL g^{-1} h^{-1} GHSV	15%	[134]
Fe_3O_4	300 °C; 0.5 MPa; 2500 mL g^{-1} h^{-1} GHSV	37.2%	[135]
1wt%Rb/Fe_3O_4	300 °C; 0.5 MPa; 2500 mL g^{-1} h^{-1} GHSV	40.8%	[135]
3wt%Rb/Fe_3O_4	300 °C; 0.5 MPa; 2500 mL g^{-1} h^{-1} GHSV	39.7%	[135]
5wt%Rb/Fe_3O_4	300 °C; 0.5 MPa; 2500 mL g^{-1} h^{-1} GHSV	38.8%	[135]
8wt%Rb/Fe_3O_4	300 °C; 0.5 MPa; 2500 mL g^{-1} h^{-1} GHSV	38.2%	[135]
Na–Fe	320 °C; 2.0 MPa; 9000 mL g^{-1} h^{-1} GHSV	25%	[136]
1Ce–Na–Fe	320 °C; 2.0 MPa; 9000 mL g^{-1} h^{-1} GHSV	27.5%	[136]
3Ce–Na–Fe	320 °C; 2.0 MPa; 9000 mL g^{-1} h^{-1} GHSV	13.6%	[136]
5Ce–Na–Fe	320 °C; 2.0 MPa; 9000 mL g^{-1} h^{-1} GHSV	23.2%	[136]
FeCe100	370 °C; 1 bar; 16 mL min^{-1} flow rate; 0.3 g_{cat}	19.5%	[137]
FeCe75Zr25	370 °C; 1 bar; 16 mL min^{-1} flow rate; 0.3 g_{cat}	24.4%	[137]
FeCe50Zr50	370 °C; 1 bar; 16 mL min^{-1} flow rate; 0.3 g_{cat}	26.6%	[137]
FeCe25Zr75	370 °C; 1 bar; 16 mL min^{-1} flow rate; 0.3 g_{cat}	22.8%	[137]
FeZr100	370 °C; 1 bar; 16 mL min^{-1} flow rate; 0.3 g_{cat}	16.9%	[137]
Fe100	370 °C; 1 bar; 16 mL min^{-1} flow rate; 0.3 g_{cat}	13.1%	[137]

2.3.3. Direct Conversion of CO_2 to HC

The hydrogenation of CO_2 to generate HC fuels involves two routes (i.e., direct and indirect routes), which are often referred to as the chemical process. The goal of producing methane and subsequent long-chain HC is the basis for the conversion of CO_2 into HC fuels. Therefore, in the energy-related scenario, the CO_2 methanation reaction has acquired remarkable interest in recent years. Indeed, it constitutes the core of the power-to-methane (PtM) process chain. This recently developed technology involves a stepwise conversion, which aims to efficiently employ the surplus energy derived from renewable power sources. The main issue of generating power from renewables is, in fact, the oscillation of electrical energy production over time [138]. This phenomenon, known as cycling, can be due to meteorological conditions, the time of day, and other aleatoric factors. The uncontrollable intermittency of power generation causes severe problems and imbalances in the power grid, making the integration of renewables harder and even less economically feasible [139]. Plenty of possible solutions to store the surplus energy have been investigated over time, resulting in the consensus that systems such as batteries and pumped-hydro systems have high capacity costs and low energy density compared to hydrocarbon [140]. Therefore, an efficient solution is to convert the surplus electrical energy into chemical energy, which can be achieved via water electrolysis. Nevertheless, the product of this conversion is hydrogen, which is a high-added-value product but presents several drawbacks, such as the difficulty in storage and transportation and the limitation on its distribution through the natural gas grid. To overcome the problem of hydrogen management, its conversion to hydrocarbons is particularly promising. In particular, CO_2 hydrogenation to methane, mostly known as CO_2 methanation, represents an attractive process to efficiently store the

surplus energy from renewables. The methane produced through this process is referred to as synthetic or substitute natural gas (SNG). It has plenty of applications, and, above all, it can be inserted into the natural gas grid without limitations [141]. Together with the advantage of being a solution for power storage, allowing the more efficient integration of renewables into the energy scenario, CO_2 methanation also has a remarkable impact on the environment from a different point of view. Indeed, it enables CO_2 consumption—for example, by employing CO_2 from sequestration systems—and can thus be considered a carbon capture and utilization (CCU) process [142,143]. Overall, the PtM process chain can be represented as in Figure 8.
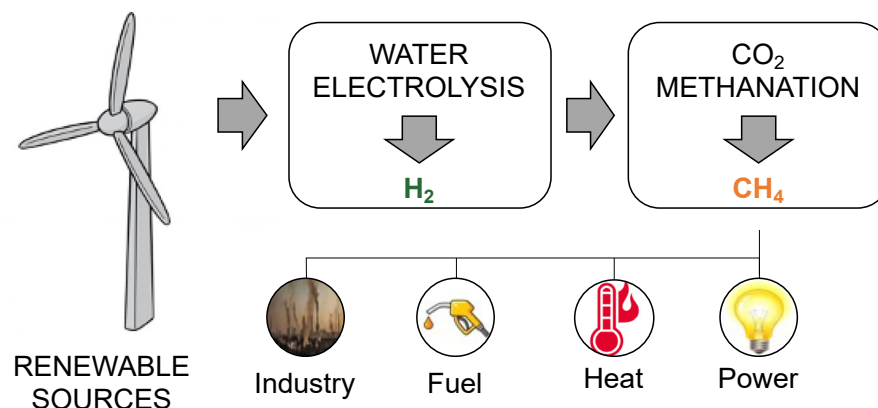

Figure 8. PtM process chain. From source to applications.

CO_2 methanation follows Equation (2), and it is an exothermic equilibrium reaction. Therefore, it presents issues related to heat management in the catalytic system, which can be summarized as follows. The heat of reaction induces a thermal gradient across the catalytic bed and occasional hotspot formation, which can be detrimental to catalyst stability, leading to sintering phenomena, reduction in the number of active sites, and loss in activity. Furthermore, the increase in local temperature represents a disadvantage for the thermodynamic equilibrium of the reaction, which is promoted at low temperatures. On the other hand, operating temperatures that are too low are detrimental to the reaction kinetics, leading to lower selectivity of the reacting system and overall lower activity.

$$CO_2 + 4H_2 \rightleftarrows CH_4 + 2H_2O \tag{2}$$

The recent attention towards CO_2 methanation drove a remarkable increase in scientific publications related to the topic in the past five years. Different catalytic formulations and catalytic systems have been explored with the aim of addressing the above-discussed issues and obtaining efficiently performing catalysts in order to allow the implementation of this process in the industrial scenario. The research approaches to the enhancement of the CO_2 methanation process can be classified as:

- Catalytic formulation optimization through the investigation of new active metals or supports;
- Utilization of structured catalysts in different shapes and materials;
- Evaluation of innovative reactor configurations (membrane reactors);
- New technologies (cold plasma reactors).

Concerning catalytic formulations, nickel is the most widely employed active species in CO_2 methanation. A comprehensive resume of the pros and cons of its application includes: its low cost and natural abundance, together with its high activity towards CO_2 activation, as the main advantages; a relatively high activation temperature, low dispersion, and reducibility as the main disadvantages [144]. Few other metals can offer the same positive characteristics as Ni; therefore, it is widely applied, and the drawbacks of its utilization are frequently compensated by support modification or a second metal addition [145].

For bimetallic formulations, Fe and Co (as transition metals) are widely reported in the literature, while, among noble metals, Ru is surely the most effective species for CO_2 methanation. In particular, it shows a relative activity higher than Ni [146] and strongly promotes the direct reaction mechanism, leading to a higher selectivity towards methane. Another basic aspect of CO_2 methanation is that a bifunctional reaction mechanism is always established: the support is involved in the reactant activation, and therefore, it plays a crucial role [147]. Plenty of studies in the literature report on the optimization of catalytic formulations, which have been recently satisfactorily reviewed [146,148–151]. Therefore, we focus on the most recent applications of engineered solutions to conduct the reaction.

Methanation over Structured Catalysts

In recent years, most of the interest has been devoted to structured catalysts. These are constituted by a carrier with a complex geometry, upon which the support and the active phases are deposited via several techniques; structured catalysts can offer several advantages for this process. First, they can be made of highly conductive materials, such as aluminum, silicon carbide, or metal alloys. The high thermal conductivity plays a fundamental role, considering the exothermicity of the reaction: indeed, these structures allow the flattening of the temperature profile within the catalytic bed, reducing the formation of hotspots and therefore the sintering phenomena and local thermodynamic limitations [152]. Furthermore, some of these structures can offer enhanced mixing characteristics, which reduce the possibility of diffusion resistance effects [94].

The most common geometrical configuration of structured catalysts is certainly the channeling structure, which is typical of honeycomb or corrugated sheet monoliths: when considering only the most conductive materials, the former are usually made of silicon carbide (SiC), while the latter are generally composed of metallic alloys; on the other hand, ceramic materials such as cordierite are frequently employed because of their ability to anchor metallic species. Indeed, NiFe/cordierite monoliths were tested in CO_2 methanation conditions in a detailed study concerning the management of the hotspot phenomena that are characteristic of this system [153]. The catalysts were obtained via in situ growth of the nanoparticles, and they were classified into high-activity and low-activity monoliths. The authors reported that low- and high-activity catalysts can be alternated over the bed, leading to a remarkably smoother increase in temperature due to the exothermic reaction, with a non-significant loss in methane yield.

Considering that Ni/CeO_2 was widely reported as one of the most promising formulations for CO_2 methanation in terms of both activity and selectivity towards methane, FeCrAlloy sheets decorated with CeO_2 nanorods to support Ni particles were recently evaluated [154]. This preparation was optimized in order to increase the stability, considering that in harsh conditions, the structured catalyst undergoes rapid deactivation. As a result, the catalysts were efficient, demonstrating higher catalytic activity compared to the powder form. Micromonoliths in commercial FeCrAlloy stainless steel were tested in CO_2 methanation with a coating of a previously optimized catalytic formulation (15 wt.% Ni, 0.5 wt.% Ru, and 10 wt.% Mg over alumina) [155]. The authors observed that the textural properties of the original powder catalysts were unchanged after deposition on the 3D structure, even though the structured catalyst exhibited sintering after the stability test. Furthermore, a noteworthy result was that transport limitations were observed at high weight hourly space velocity (WHSV) conditions, which can be ascribable to the channeling structure. Indeed, the same kind of 3D structure obtained with aluminum sheets was employed with a Ni/CeO_2 coating with a variety of configurations (plain, stacked, segment, and multi-stacked), proving that avoiding a channeling flow regime is beneficial for the reaction [156]. This conclusion is further upheld by comparative studies that involve channeling structures (such as honeycomb monoliths) and randomly organized structures (open-cell foams). The comparison between an alumina open-cell foam and a cordierite monolith highlighted that the external mass transfer is maximized in the case of the open-cell foam thanks to its characteristic irregular structure, which ensures a more

intimate contact between phases [157]. In particular, the light-off temperature (which is a typical parameter to be taken into account in CO_2 methanation and can be considered the temperature at which the reaction starts—i.e., it has a significant conversion) was found to be remarkably lower in the foam catalytic system. The same result in terms of optimized heat and mass transfer was observed through a comparison between an aluminum open-cell foam and a SiC monolith, with the foam-supported catalyst showing the best performance in terms of methane yield and light-off temperature [158]. CO_2 methanation was also investigated over high-pore-density (75 ppi—*pores per inch*) metallic (Ni) foams, which were coated with CeO_2 (via electrodeposition) and impregnated with Ru [159]. The high pore density of the carrier and the low thickness of the coating produced outstanding transport properties, suggesting that this catalyst is particularly suitable for the process intensification of highly exothermic catalytic reactions.

The importance of the thermal conductivity of the carrier was evaluated with a comparison between two 40 PPI open-cell foams, one made of alumina (low conductivity) and one made of SiC (high conductivity) [160]. Activity tests were performed in a bench-scale reactor with an integrated cooling system in order to evaluate the effect of co-current or counter-current refrigeration of the system. The use of carriers having similar geometrical and morphological properties is particularly significant to the aim of discerning the thermal conductivity effect; therefore, the outcomes of this evaluation offer a noteworthy perspective in the application of highly conductive structured catalysts. The results showed that, as expected, the SiC foam offered a flatter thermal profile, which is beneficial from a thermodynamic perspective. Furthermore, with the Al_2O_3-based catalyst, the difficulty of removing heat with the refrigerating medium was ascribed to the radial heat transfer resistance.

According to this result, a simulation study of CO_2 methanation over ceramic paper catalysts revealed that the most relevant contribution to the effective heat transfer is the radial heat dispersion through conduction; in contrast, the dynamic contributions are not significant, considering the low linear gas velocity [161].

Due to the remarkable enhancement of reaction performance in the presence of random 3D structures, research has been devoted to the reproduction of ordered geometries with the same properties. This result was achieved through additive manufacturing (AM). Regular periodic 3D structures with two different layer stacking configurations were tested for CO_2 methanation applications [162]. The best results were obtained with the "zig-zag" layer organization, which allowed improved heat and mass transfer. Furthermore, with the optimized configuration, it was also observed that stainless steel is a beneficial material for ensuring a better coating adhesion compared to copper [163].

Innovative Reactor Configurations

The most consolidated solution to conduct CO_2 methanation is surely the adiabatic fixed-bed reactor or cooled fixed-bed reactors. The former can be operated with inter-stage cooling, even though this solution requires many auxiliary units (heat exchanger). The latter, instead, is a more compact solution; however, the temperature and pressure drop control is more complicated. Other solutions, such as fluidized bed reactors and microchannels reactors, are still in the early stage of research. The interest towards microchannel reactors is mainly related to the possibility of having a mass transfer completely dominated by diffusion, as the normal velocity with respect to the surface is almost null. Fuentes et al. [164] simulated a microchannel system and showed that with a large number of channels having a small cross-sectional area, the prevalence of diffusive forces could be increased. These enhance methane production, and therefore, the resulting product stream is more suitable for insertion in the natural gas infrastructure.

The integration of membrane technology with a catalytic reaction always draws remarkable attention in terms of process intensification, as it can enhance the catalytic performance over the thermodynamic equilibrium. Their application is frequently intended to remove a product from the catalytic zone in order to force the reaction equilibrium

towards the products. In methanation systems, membrane reactors could be applied for water removal but also for a local supply of hydrogen, and vice versa.

In situ water removal in CO_2 methanation systems theoretically provides 100% conversion of CO_2 when water is completely removed (R = 0.99) at any temperature, pressure, or CH_4/CO_2 ratio [165]. For water separation, hydrophilic membranes are applied. The main drawback is that non-condensable gases pass through the membrane via the Knudsen diffusion mechanism, even though their permeability is reduced by progressively increasing water capillary condensation. The first attempt to employ a membrane reactor for the Sabatier process was performed in 1997 with a water-permeable membrane: as a result, an increase in CO_2 conversion of 18% was obtained with the integrated system compared to the conventional fixed-bed reactor [166]. Experimental data of integrated systems available in the literature were successfully approximated by a simulation in which a water-permeable hydroxy sodalite (H-SOD) membrane and H_2 as the sweep gas were considered [167]. Hydrogen was employed because it minimizes the reactant loss and maximizes the product permeation. The simulations indicated that enhanced conversion could be obtained in mild temperature and pressure conditions, which potentially represent a lower operating expense (OPEX). Furthermore, a more in-depth evaluation in a 2D simulation study demonstrated that the highest permeation flux was established at the inlet, while the outlet was characterized by a balance between H_2O permeation and the production rate [168]. Nevertheless, the simulation results showed a 90% water removal and an 8.3% CO_2 conversion increase. As an outcome, since the reaction rate was found to be much higher than water permeation, the authors concluded that for reactors with high GHSVs, the utilization of membranes with high water permeance is mandatory.

The introduction of a hydrogen-permeable membrane in CO_2 methanation systems is an attractive alternative for the coupling of different processes. An example was provided by Miyamoto et al. [169], who integrated NH_3 decomposition, which provides hydrogen, with CO_2 methanation. Therefore, hydrogen was removed from the first reaction system and supplied to the second by a Pd membrane, with the obtainment of a significant increase in both NH_3 decomposition and H_2 separation. Nevertheless, the local supply of hydrogen was not effective in improving the methanation rate, as it was found to be comparable to the value obtained in the packed-bed reactor; on the other hand, CH_4 selectivity was increased, resulting in an enhancement of reaction performance. A coupled system of dehydrogenation/hydrogenation reactions was also proposed by Bian et al. [170] in their CFD simulation. Cyclohexane dehydrogenation was considered at the retentate side, while CO_2 methanation was set at the permeate side. This study supports the previously reported result that a high-permeance membrane is mandatory in order to enhance the performance of both reactions.

CO$_2$ Methanation under NTP Process

The interest towards non-thermal plasma (NTP) applications in methanation processes is primarily related to the main reactant activation. Indeed, CO_2 is a highly stable molecule, and therefore, in conventional catalytic systems, C=O bond breakage is promoted with the use of suitable active species (Ni or Ru, for example); furthermore, each catalytic formulation has its own light-off temperature, which is just below 200 °C. When plasma is applied, high-energy species such as free radicals and ions are involved, and these species can activate CO_2 molecules without the necessity of external heating. In NTP technology, several configurations can be realized, although the most employed solution is represented by the dielectric barrier discharge (DBD) reactor [110]. The application of NTP to CO_2 methanation is a remarkably recent topic; nevertheless, several catalytic systems have been evaluated under plasma conditions. Plasma is particularly useful for the removal of water molecules from the catalytic surface: this was specifically observed over Si/Al zeolite-supported catalysts in a DBD reactor [171]. Furthermore, as NTP is expected to reduce the reaction barrier thanks to its non-equilibrium nature, it potentially allows performing the reaction without a catalyst. The study conducted by Ahmad et al. [172] was indeed focused

on a plasma-Ni system. The authors considered the NTP + Ni catalyst hybrid system and compared it with a Ni catalyst in a thermal (Ni-T) system and an NTP-driven reaction. As outcomes, the plasma-assisted system allowed consistent methane selectivity at a remarkably low temperature (150 °C). The hybrid plasma–catalytic system compared to the thermal–catalytic system resulted in a CO_2 conversion 20 times higher and a CH_4 selectivity 5 times higher than the Ni–T configuration. Non-thermal plasma was also evaluated in the presence of more complex catalytic formulations (hydrotalcite-derived catalysts with Ni–Fe active species) with satisfactory results, suggesting its suitability in dynamic systems working with excess energy [173]. Even though the NTP is a low-temperature technology, the exothermicity of CO_2 methanation cannot be neglected. The study of Bosét-Peiró et al. [174] showed that a pseudo-adiabatic plasma-assisted configuration could reach an energy efficiency of 73%, and therefore, the overall process is undeniably less energetically demanding. A combination of non-thermal plasma technology and a structured catalyst was evaluated by Gao et al. [175], who performed a complex study related to the mechanisms in plasma-assisted CO_2 methanation. The authors observed that the system is structure-dependent, as different structures led to different CH_4 selectivities due to the dissimilar discharges within the catalytic bed. Furthermore, the mechanistic study highlighted that, due to the plasma presence, several radicals were formed in the system (CO, CO(v), H, and H(v)). In particular, CO(v_1) was individuated as the main vibrational state, resulting in a reduced energy barrier and, therefore, in a lower activation temperature. The short-term stability under NTP conditions was recently evaluated by the same authors over a Ni–Y/CeO_2 formulation, showing excellent stability for 12 h and remarkable catalytic activity with a CO_2 conversion of 84% and selectivity to methane of 83% [176].

Industrial Applications and Outlook

CO_2 hydrogenation to methane is a captivating topic in several fields, ranging from CO_2 utilization to methane production and renewable inclusion in power generation technologies. This new concept has been widely studied in recent years, leading to the obtainment of a mature technology, at least for thermo-catalytic CO_2 methanation. Germany can be regarded as the leader in PtM technology: in Stuttgard and in Wertle, two power-to-methane plants (with capacities of 250 kW and 6300 kW power input, respectively) produce methane for Audi. Furthermore, Germany is also at the cutting edge of biological methanation technologies, with the first commercial-scale project with a 1 MW capacity [148]. Innovative solutions such as structured catalysts, membrane reactors, and plasma-assisted systems are, therefore, highly promising for the industrial scenario, as they represent possible solutions for the intensification of this newborn process, aiming to further enhance energy efficiency. The most relevant findings related to these innovative applications and reviewed in this work are summarized in Table 7.

Table 7. Summary of the most recent relevant findings in CO_2 methanation reported in this review.

Technology	Catalyst	Study Outcomes	Ref.
Structured catalysts	NiFe/cordierite monoliths	Low- and high-activity catalysts can be conveniently alternated over the bed to smooth the temperature increase due to the reaction	[153]
	FeCrAlloy sheets + CeO_2 nanoroads	Highly active and selective compared to the powder catalysts	[153]
	FeCrAlloy micro-monoliths with 15 wt.% Ni, 0.5 wt.% Ru, and 10 wt.% Mg	The structured catalyst exhibited sintering but no changes in textural properties. High WHSV led to transport limitations due to the channeling structure	[155]
	Al sheet with Ni/CeO_2 coating	Avoiding channeling flow regime is beneficial for the reaction	[156]
	Alumina open-cell foam and cordierite monolith	External mass transfer is maximized for the open-cell foam	[157]

Table 7. *Cont.*

Technology	Catalyst	Study Outcomes	Ref.
	Aluminum open-cell foams and SiC monolith	Foams provide the best methane yield and light-off temperature	[158]
	Ni foams coated with CeO_2	Outstanding transport properties thanks to low coating thickness and high pore density of the foam	[159]
	Alumina and SiC open-cell foams	SiC foam offered a flatter thermal profile and allowed easier heat removal	[160]
	SS-AM catalysts	The "zig-zag" organization allowed improved heat and mass transfer	[162]
	SS and copper AM catalysts	SS ensures better coating adhesion and therefore better catalytic activity	[163]
Microchannel reactors	(Simulation study)	Methane production can be enhanced by many channels having small cross-sectional area, which increase diffusion	[164]
	(Simulation study)	100% CO_2 conversion when water removal efficiency is 0.99	[165]
H_2O-permeable membrane	-	Increase in CO_2 conversion of 18% with the membrane reactor	[166]
	-	Water-permeable H-SOD membrane enhances CO_2 conversion and potentially reduces OPEX	[167]
	(Simulation study)	90% water removal induces an 8.3% increase in CO_2 conversion	[168]
H_2 permeable membrane	-	Coupling of NH_3 decomposition with CO_2 methanation: the system has outstanding CH_4 selectivity even though the H_2 supply was too low; therefore, the overall reaction rate is comparable to a packed-bed reactor system	[169]
	-	Cyclohexane dehydrogenation coupled with CO_2 methanation: the higher the membrane permeance, the higher the enhancement of both reactions	[170]
	Si/Al zeolite	Plasma is particularly useful for removing water molecules from the catalyst surface	[171]
	Ni catalyst	The hybrid plasma–Ni system offered a CO_2 conversion 20 times higher and a CH_4 selectivity 5 times higher than the thermal–Ni system	[172]
NTP	-	Pseudo-adiabatic plasma-assisted system could exploit the exothermicity of the process, yielding an energy efficiency of 73%	[174]
	-	The system is structure-dependent: different catalyst structures give different CH_4 selectivities due to dissimilar discharges within the bed	[175]
	Ni-Y/CeO_2	Excellent stability of the plasma-assisted system for 12 h, with CO_2 conversion of 84% and CH_4 selectivity of 83%	[176]

3. Conclusions

In recent years, a progressively different approach to the generation of power and the production of fuels for the automotive sector as well as for domestic applications has been taken. This is mainly driven by increasing environmental concerns, and it is directly translated into research on the feasibility of applying renewable energy sources to the present energy scenario and into the reduction of greenhouse gas emissions. Following more than one approach, the integration of renewables mainly involves the utilization of biomass-derived raw material and the combination of power generated via clean sources with conventional power generation systems. The aim of this review article was to provide a satisfactory overview of the most recent solutions to the above-discussed issues.

One of the greatest challenges of the modern era is certainly the substitution of natural gas (methane) with biomass-derived materials, thereby decreasing the depletion of fossil fuels and increasing the sustainability of several industrial processes. Among them, the reforming process has doubtlessly received most of the attention, as it allows the synthesis of hydrogen, which is considered the energy carrier of the future. The substitution of methane with a biomass-derived material leads to the production of "green hydrogen".

The most attractive alternative to methane in reforming processes is certainly bioethanol, a widely available renewable source. In the context of bioethanol reforming, several studies have recently been published to address the main obstacle to wider diffusion, i.e., catalyst deactivation due to coke formation. Attention has been mainly focused on the utilization of highly active catalytic systems (based on noble metals) that are selective and resistant to deactivation; furthermore, the use of promoters and bimetallic catalytic systems has led to enormous improvements in the performance of nickel-based catalytic systems, which are the most frequently used. The use of conductive structured catalysts has also improved heat transfer rates and reduced mass transfer limitations, thus allowing the optimization of reactor sizes and the heat supply. However, in order to produce high-purity hydrogen, the syngas obtained from bioethanol reforming must be further treated. The purification stages could be considered the real bottleneck of the whole hydrogen production process, and their impact dramatically increases in the case of on-site H_2 production. The water–gas shift reaction is the most consolidated technology for syngas cleaning; therefore, the intensification of this process is currently widely investigated. Many published works have focused on the improvement of conventionally used catalytic systems for LTS and HTS processes; however, real intensification can only be achieved by designing a single-stage process integrated with a membrane separation system. Extremely promising are studies on a medium-high temperature WGS process, in which the thermal profile of the catalyst is flattened by the presence of conductive structures, integrated with a Pd–Cu catalytic membrane for the separation of hydrogen or with a ceramic−carbonate dual-phase membrane to obtain high-purity CO_2. However, further studies are needed to improve the efficiency performance of available membranes.

On the other hand, the reduction in greenhouse gas emissions mainly focuses on the emissions of CO_2. Several solutions have been explored in this field, such as CCS and CCU systems, with the latter being the most promising. Indeed, plenty of studies have reported on hydrogenation processes to produce fine chemicals and fuels. Different paths can be followed to obtain methane (which also represents a substitute natural gas), methanol, or hydrocarbons via the Fischer–Tropsch process. In this regard, particularly interesting are studies on the use of non-thermal plasma-assisted systems, in which the reaction barrier can be reduced by exploiting the non-equilibrium nature of the process. These hydrogenation processes are encouraged by the use of sustainable hydrogen, thus producing H_2 via water electrolysis, thermolysis, biomass gasification, biocatalysis, and fermentation. This sustainable hydrogen represents a power storage technology, and its utilization is a way to integrate renewables into the power generation scenario. In conclusion, the watchword is "renewable", and the key is "hydrogen": hydrogen as an energy carrier obtained from renewable sources and using renewable energy, and renewable hydrogen to sequester CO_2 and obtain useful chemicals.

Abbreviation

AM   Additive manufacturing
CCU   Carbon capture and utilization
CTLO CO_2 hydrogenation to lower olefins
DBD   Dielectric barrier discharges
DFT   Density functional theory
FTS   Fischer–Tropsch synthesis
GHSV   Gas hourly space velocity
HC   Hydrocarbons
H-SOD   Hydroxy sodalite
HTS   High-temperature shift
LTS   Low-temperature shift
MTO   Methanol conversion to olefins
NTP   Non-thermal plasma
OPEX   Operating expenses
ppi   Pores per inch
PPI   Process intensification
PtM   Power-to-methane
RWGS   Reverse water–gas shift
SBA   Santa Barbara amorphous
SNG   Synthetic (or substitute) natural gas
WGS   Water–gas shift
WHSV   Weight hourly space velocity

References

1. The Paris Agreement. Available online: https://www.un.org/en/climatechange/paris-agreement (accessed on 18 February 2022).
2. Soltani, S.M.; Lahiri, A.; Bahzad, H.; Clough, P.; Gorbounov, M.; Yan, Y. Sorption-enhanced Steam Methane Reforming for Combined CO_2 Capture and Hydrogen Production: A State-of-the-Art Review. *Carbon Capture Sci. Technol.* **2021**, *1*, 100003. [CrossRef]
3. Martino, M.; Ruocco, C.; Meloni, E.; Pullumbi, P.; Palma, V. Main Hydrogen Production Processes: An Overview. *Catalysts* **2021**, *11*, 547. [CrossRef]
4. Safari, F.; Dincer, I. A review and comparative evaluation of thermochemical water splitting cycles for hydrogen production. *Energy Convers. Manag.* **2020**, *205*, 112182. [CrossRef]
5. Yan, Y.; Thanganadar, D.; Clough, P.T.; Mukherjee, S.; Patchigolla, K.; Manovic, V.; Anthony, E.J. Process simulations of blue hydrogen production by upgraded sorption enhanced steam methane reforming (SE-SMR) processes. *Energy Convers. Manag.* **2020**, *222*, 113144. [CrossRef]
6. van Renssen, S. The hydrogen solution? *Nat. Clim. Chang.* **2020**, *10*, 799–801. [CrossRef]
7. European Commission. *Europe's Moment: Repair and Prepare for the Next Generation*; European Commission: Bruxelles, Belgium, 2020.
8. Anastas, P.T.; Warner, J.C. *Green Chemistry: Theory and Practice*; Oxford University Press: New York, NY, USA, 1998.
9. Sheldon, R.A. Engineering a more sustainable world through catalysis and green chemistry. *J. R. Soc. Interface* **2016**, *13*, 20160087. [CrossRef] [PubMed]
10. Huang, Y.; Wang, B.; Yuan, H.; Sun, Y.; Yang, D.; Cui, X. The catalytic dehydrogenation of ethanol by heterogeneous catalysts. *Catal. Sci. Technol.* **2021**, *11*, 1652–1664. [CrossRef]
11. Constable, D.J.C. Green and sustainable chemistry—The case for a systems-based, interdisciplinary approach. *iScience* **2021**, *24*, 103489. [CrossRef] [PubMed]
12. Kumar, A. Ethanol Decomposition and Dehydrogenation for Hydrogen Production: A Review of Heterogeneous Catalysts. *Ind. Eng. Chem. Res.* **2021**, *60*, 16561–16576.
13. Sanchez, N.; Ruiz, R.Y.; Infante, N.; Cobo, M. Bioethanol Production from Cachaza as Hydrogen Feedstock: Effect of Ammonium Sulfate during Fermentation. *Energies* **2017**, *10*, 2112.
14. Domínguez, M.; Taboada, E.; Molins, E.; Llorca, J. Co-Fe-Si Aerogel Catalytic Honeycombs for Low Temperature Ethanol Steam Reforming. *Catalysts* **2012**, *2*, 386–399.
15. Song, J.H.; Yoo, S.; Yoo, J.; Park, S.; Gim, M.Y.; Kim, T.H.; Song, I.K. Hydrogen production by steam reforming of ethanol over Ni/Al2O3-La2O3 xerogel catalysts. *Mol. Catal.* **2017**, *434*, 123–133.
16. Palma, V.; Ruocco, C.; Meloni, E.; Ricca, A. Influence of Catalytic Formulation and Operative Conditions on Coke Deposition over CeO2-SiO2 Based Catalysts for Ethanol Reforming. *Energies* **2017**, *10*, 1030.
17. Pio, G.; Ruocco, C.; Palma, V.; Salzano, E. Detailed kinetic mechanism for the hydrogen production via the oxidative reforming of ethanol. *Chem. Eng. Sci.* **2021**, *237*, 116591.

18. Palma, V.; Ruocco, C.; Cortese, M.; Martino, M. Bioalcohol Reforming: An Overview of the Recent Advances for the Enhancement of Catalyst Stability. *Catalysts* **2020**, *10*, 665.

19. Palma, V.; Ruocco, C.; Ricca, A. Ceramic foams coated with PtNi/CeO2ZrO2 for bioethanol steam reforming. *Int. J. Hydrog. Energy* **2016**, *41*, 11526–11536.

20. Sanchez, N.; Ruiz, R.; Hacker, V.; Cobo, M. Impact of bioethanol impurities on steam reforming for hydrogen production: A review. *Int. J. Hydrog. Energy* **2020**, *45*, 11923–11942.

21. Cifuentes, B.; Gómez, J.; Sánchez, N.; Proaño, L.; Bustamante, F.; Cobo, M. Bioethanol steam reforming over monoliths washcoated with RhPt/CeO2–SiO2: The use of residual biomass to stably produce syngas. *Int. J. Hydrog. Energy* **2021**, *46*, 4007–4018.

22. Sharma, Y.C.; Kumar, A.; Prasad, R.; Upadhyay, S.N. Ethanol steam reforming for hydrogen production: Latest and effective catalyst modification strategies to minimize carbonaceous deactivation. *Renew. Sustain. Energy Rev.* **2017**, *74*, 89–103.

23. Ogo, S.; Sekine, Y. Recent progress in ethanol steam reforming using non-noble transition metal catalysts: A review. *Fuel Process. Technol.* **2020**, *199*, 106238.

24. Ferreira, N.; Coronel, L.; Moreno, M.S.; Cornaglia, L.M.; Múnera, J.F. Active and stable Co catalysts supported on La-Si binary systems for H2 production through ethanol steam reforming. *Fuel Process. Technol.* **2021**, *217*, 106814.

25. Liu, H.; Li, H.; Li, S. Ni-hydrocalumite derived catalysts for ethanol steam reforming on hydrogen production. *Int. J. Hydrog. Energy* **2021**, *7*, 141.

26. Efimov, M.N.; Mironova, E.Y.; Vasilev, A.A.; Muratov, D.G.; Zhilyaeva, N.A.; Ozkan, S.Z.; Karpacheva, G.P. Comparison of bimetallic Co-Ru nanoparticles supported on highly porous activated carbonized polyacrylonitrile with monometallic ones in ethanol steam reforming. *J. Environ. Chem. Eng.* **2021**, *9*, 106429.

27. Greluk, M.; Gac, W.; Rotko, M.; Słowik, G.; Turczyniak-Surdacka, S. Co/CeO2 and Ni/CeO2 catalysts for ethanol steam reforming: Effect of the cobalt/nickel dispersion on catalysts properties. *J. Catal.* **2021**, *393*, 159–178.

28. Pizzolitto, C.; Menegazzo, F.; Ghedini, E.; Martínez Arias, A.; Cortés Corberán, V.; Signoretto, M. Microemulsion vs. Precipitation: Which Is the Best Synthesis of Nickel–Ceria Catalysts for Ethanol Steam Reforming? *Processes* **2021**, *9*, 77.

29. Valecillos, J.; Iglesias-Vázquez, S.; Landa, L.; Remiro, A.; Bilbao, J.; Gayubo, A.G. Insights into the Reaction Routes for H2 Formation in the Ethanol Steam Reforming on a Catalyst Derived from NiAl2O4 Spinel. *Energy Fuels* **2021**, *35*, 17197–17211.

30. Musso, M.; Cardozo, A.; Romero, M.; Faccio, R.; Segobia, D.; Apesteguía, C.; Bussi, J. High performance Ni-catalysts supported on rare-earth zirconates (La and Y) for hydrogen production through ethanol steam Characterization and assay. *Catal. Today.* in press. [CrossRef]

31. Zhurka, M.D.; Lemonidou, A.A.; Kechagiopoulos, P.N. Elucidation of metal and support effects during ethanol steam reforming over Ni and Rh based catalysts supported on (CeO2)-ZrO2-La2O3. *Catal. Today* **2020**, *368*, 161–172.

32. Martínez, A.H.; Lopez, E.; Cadús, L.E.; Agüero, F.N. Elucidation of the role of support in Rh/perovskite catalysts used in ethanol steam reforming reaction. *Catal. Today* **2021**, *372*, 59–69.

33. Boudadi, K.; Bellifa, A.; Márquez-Álvarez, C.; Cortés Corberán, V. Nickel catalysts promoted with lanthanum for ethanol steam reforming: Influence of support and treatment on activity. *Appl. Catal. A Gen.* **2021**, *619*, 118141.

34. Rajabi, Z.; Jones, L.; Martinelli, M.; Qian, D.; Cronauer, D.C.; Kropf, A.J.; Watson, C.D.; Jacobs, J. Influence of Cs Promoter on Ethanol Steam-Reforming Selectivity of Pt/m-ZrO2 Catalysts at Low Temperature. *Catalysts* **2021**, *11*, 1104.

35. Martinelli, M.; Castro, J.D.; Alhraki, N.; Matamoros, M.E.; Kropf, A.J.; Cronauer, D.C.; Jacobs, G. Effect of sodium loading on Pt/ZrO2 during ethanol steam reforming. *Appl. Catal. A Gen.* **2021**, *610*, 117947.

36. Martinelli, M.; Garcia, R.; Watson, C.D.; Cronauer, D.C.; Kropf, A.J.; Jacobs, G. Promoting the Selectivity of Pt/m-ZrO2 Ethanol Steam Reforming Catalysts with K and Rb Dopants. *Nanomaterials* **2021**, *11*, 2233. [PubMed]

37. Matus, E.; Sukhova, O.; Ismagilov, I.; Kerzhentsev, M.; Stonkus, O.; Ismagilov, Z. Hydrogen Production through Autothermal Reforming of Ethanol: Enhancement of Ni Catalyst Performance via Promotion. *Energies* **2021**, *14*, 5176.

38. An, X.; Feng, C.; Ren, J.; Shi, K.; Du, Y.; Xie, X.; Wu, X. Novel highly dispersed Ni-based oxides catalysts for ethanol steam reforming. *J. Energy Inst.* **2021**, *99*, 240–247.

39. Ito, S.-. i Kameoka, S. Effect of strong metal-oxide interaction on low-temperature ethanol reforming over Fe-promoted Rh/SiO2 catalyst. *Appl. Catal. A Gen.* **2021**, *617*, 118113.

40. Wu, Y.; Pei, C.; Tian, H.; Liu, T.; Zhang, X.; Chen, S.; Xiao, Q.; Wang, X.; Gong, J. Role of Fe Species of Ni-Based Catalysts for Efficient Low-Temperature Ethanol Steam Reforming. *JACS Au* **2021**, *1*, 1459–1470.

41. Zanchet, D.; Santos, J.B.O.; Damyanova, S.; Gallo, J.M.R.; Bueno, J.M.C. Toward Understanding Metal-Catalyzed Ethanol Reforming. *ACS Catal.* **2015**, *5*, 3841–3863.

42. Ni, M.; Leung, D.; Leung, M. A review on reforming bio-ethanol for hydorgen production. *Int. J. Hydrog. Energy* **2007**, *32*, 3238–3247. [CrossRef]

43. Gu, T.; Zhu, W.; Yang, B. Ethanol steam reforming on Rh: Microkinetic analyses on the complex reaction network. *Catal. Sci. Technol.* **2021**, *11*, 7009–7017.

44. Martinelli, M.; Watson, C.D.; Jacobs, G. Sodium doping of Pt/m-ZrO2 promotes C–C scission and decarboxylation during ethanol steam reforming. *Int. J. Hydrog. Energy* **2020**, *45*, 18490–18501.

45. Hamryszak, A.; Madej-Lachowska, M.; Kulawska, M.; Ruggiero-MikoBajczyk, M.; Samson, K.; Zliwa, M. Investigation on binary copper-based catalysts used in the ethanol steam reforming process. *React. Kinet. Mech. Catal.* **2020**, *130*, 727–739.

46. Palma, V.; Ruocco, C.; Castaldo, F.; Ricca, A.; Boettge, D. Ethanol steam reforming over bimetallic coated ceramic foams: Effect of reactor configuration and catalytic support. *Int. J. Hydrog. Energy* **2015**, *40*, 12650–12662.

47. Belzunce, P.S.; Cadús, L.E.; Rodríguez, M.L. Cross-flow plate reactor for ethanol steam reforming: A theoretical study. *Chem. Eng. Process.—Process. Intensif.* **2021**, *164*, 108383.

48. Escalante, Y.; Galetti, A.E.; Gómez, M.F.; Furlong, O.J.; Nazzarro, M.S.; Barroso, M.N.; Abello, M.C. Hydrogen production by ethanol steam reforming: A study of Co- and Ce-based catalysts over FeCrAlloy monoliths. *Int. J. Hydrog. Energy* **2020**, *45*, 20956–20969.

49. Ruocco, C.; Palma, V.; Cortese, M.; Martino, M. Stability of bimetallic Ni/CeO2–SiO2 catalysts during fuel grade bioethanol reforming in a fluidized bed reactor. *Renew. Energy* **2022**, *182*, 913–922.

50. Jia, H.; Xu, H.; Sheng, X.; Yang, X.; Shen, W.; Goldbach, A. High-temperature ethanol steam reforming in PdCu membrane reactor. *J. Membr. Sci.* **2020**, *605*, 118083.

51. Eremeev, N.; Krasnov, A.; Bespalko, Y.; Bobrova, L.; Smorygo, O.; Sadykov, V. An Experimental Performance Study of a Catalytic Membrane Reactor for Ethanol Steam Reforming over a Metal Honeycomb Catalyst. *Membranes* **2021**, *11*, 790. [PubMed]

52. Phung, T.K.; Le Minh Pham, T.; Nguyen, A.; Vu, K.; Giang, H.N.; Nguyen, T.; Cong Huynh, T.C.; Pham, D. Effect of Supports and Promoters on the Performance of Ni-Based Catalysts in Ethanol Steam Reforming. *Chem. Eng. Technol.* **2020**, *42*, 672–688. [CrossRef]

53. Palma, V.; Ruocco, C.; Meloni, E.; Rivva, A. Oxidative reforming of ethanol over CeO2-SiO2 based catalysts in a fluidized bed reactor. *Chem. Eng. Process. Process. Intensif.* **2018**, *124*, 319–327. [CrossRef]

54. Roldan, R. Technical and economic feasibility of adapting an industrial steam reforming unit for production of hydrogen from renewable ethanol. *Int. J. Hydrog. Energy* **2015**, *40*, 2035–2046. [CrossRef]

55. Palma, V.; Ruocco, C.; Cortese, M.; Renda, S.; Meloni, E.; Festa, G.; Martino, M. Platinum Based Catalysts in the Water Gas Shift Reaction: Recent Advances. *Metals* **2020**, *10*, 866. [CrossRef]

56. Chen, W.-H.; Chen, C.-Y. Water gas shift reaction for hydrogen production and carbon dioxide capture: A review. *Appl. Energy* **2020**, *258*, 114078. [CrossRef]

57. Bang, G.; Moon, D.-K.; Kang, J.-H.; Han, Y.-J.; Kim, K.-M.; Lee, C.-H. High-purity hydrogen production via a water-gas-shift reaction in a palladium-copper catalytic membrane reactor integrated with pressure swing adsorption. *Chem. Eng. J.* **2021**, *411*, 128473. [CrossRef]

58. Pal, D.; Chand, R.; Upadhyay, S.; Mishra, P.K. Performance of water gas shift reaction catalysts: A review. *Renew. Sustain. Energy Rev.* **2018**, *93*, 549–565.

59. Zhu, M.; Wachs, I.E. Iron-Based Catalysts for the High-Temperature Water–Gas Shift (HT-WGS) Reaction: A Review. *ACS Catal.* **2015**, *6*, 722–732.

60. Zhang, Z.; Chen, X.; Kang, J.; Yu, Z.; Tian, J.; Gong, Z.; Jia, A.; You, R.; Qian, K.; He, S.; et al. The active sites of Cu–ZnO catalysts for water gas shift and CO hydrogenation reactions. *Nat. Commun.* **2021**, *12*, 4331. [CrossRef] [PubMed]

61. Dong, Z.; Liu, W.; Zhang, L.; Wang, S.; Luo, L. Structural Evolution of Cu/ZnO Catalysts during Water-Gas Shift Reaction: An In Situ Transmission Electron Microscopy Study. *ACS Appl. Mater. Interfaces* **2021**, *13*, 41707–41714. [CrossRef]

62. Bian, Z.; Zhong, W.; Yu, Y.; Jiang, B.; Kawi, S. Cu/SiO2 derived from copper phyllosilicate for lowtemperature water-gas shift reaction: Role of Cu$^+$ sites. *Int. J. Hydrog. Energy* **2020**, *45*, 27078–27088. [CrossRef]

63. Salcedo, A.; Irigoyen, B. Unraveling the Origin of Ceria Activity in Water−Gas Shift by First Principles Microkinetic Modeling. *J. Phys. Chem. C* **2020**, *124*, 7823–7834. [CrossRef]

64. Lee, Y.-H.; Kim, H.-M.; Jeong, C.-H.; Jeong, D.-W. Effects of precipitants on the catalytic performance of Cu/CeO2 catalysts for the water–gas shift reaction. *Catal. Sci. Technol.* **2021**, *11*, 6380. [CrossRef]

65. Yu, W.-Z.; Wang, W.-W.; Ma, C.; Li, S.-Q.; Wu, K.; Zhu, J.-Z.; Zhao, H.-R.; Yan, C.-H.; Jia, C.-J. Very high loading oxidized copper supported on ceria to catalyze the water-gas shift reaction. *J. Catal.* **2021**, *402*, 83–93. [CrossRef]

66. Ning, J.; Zhou, Y.; Shen, W. Atomically dispersed copper species on ceria for the low-temperature water-gas shift reaction. *Sci. China Chem.* **2021**, *64*, 1103–1110. [CrossRef]

67. Liang, J.-X.; Lin, J.; Liu, J.; Wang, X.; Zhang, T.; Li, J. Dual Metal Active Sites in an Ir1/FeOx Single-Atom Catalyst: A Redox Mechanism for the Water-Gas Shift Reaction. *Angew. Chem. Int. Ed.* **2020**, *59*, 12868–12875. [CrossRef]

68. Sun, L.; Xu, J.; Liu, X.; Qiao, B.; Li, L.; Ren, Y.; Wan, Q.; Lin, J.; Lin, S.; Wang, X.; et al. High-Efficiency Water Gas Shift Reaction Catalysis on α-MoC Promoted by Single-Atom Ir Species. *ACS Catal.* **2021**, *11*, 5942–5950. [CrossRef]

69. Ariëns, M.I.; Chlan, V.; Novák, P.; van de Water, L.G.A.; Dugulan, A.I.; Brück, E.; Hensen, E.J.M. The role of chromium in iron-based high-temperature water-gas shift catalysts under industrial conditions. *Appl. Catal. B-Environ.* **2021**, *297*, 120465. [CrossRef]

70. Yalcin, O.; Wachs, I.E.; Onal, I. Role of chromium in Cr–Fe oxide catalysts for high temperature water-gas shift reaction—A DFT study. *Int. J. Hydrog. Energy* **2021**, *46*, 17154–17162. [CrossRef]

71. Ratnasamy, C.; Wagner, J.P. Water Gas Shift Catalysis. *Catal. Rev.* **2009**, *51*, 325–440. [CrossRef]

72. Polo-Garzon, F.; Fung, V.; Nguyen, L.; Tang, Y.; Tao, F.; Cheng, Y.; Daemen, L.L.; Ramirez-Cuesta, R.-C.; Foo, G.S.; Zhu, M.; et al. Elucidation of the Reaction Mechanism for High-Temperature Water Gas Shift over an Industrial-Type Copper−Chromium−Iron Oxide Catalyst. *J. Am. Chem. Soc.* **2019**, *141*, 7990–7999. [CrossRef]

73. Ariëns, M.I.; van de Water, L.G.A.; Dugulan, A.I.; Brück, E.; Hensen, E.J.M. Copper promotion of chromium-doped iron oxide water-gas shift catalysts under industrially relevant conditions. *J. Catal.* **2022**, *405*, 391–403. [CrossRef]

74. Damma, D.; Welton, A.; Boolchand, P.; Dong, J.; Smirniotis, P.G. Ce/Cr and Ce/Co modified ferrite catalysts for high temperature water-gas shift reaction at elevated pressures. *J. Catal.* **2022**, *405*, 35–46. [CrossRef]

75. Popovic, J.; Lindenthal, L.; Rameshan, R.; Ruh, T.; Nenning, A.; Löffler, S.; Opitz, A.K.; Rameshan, C. High Temperature Water Gas Shift Reactivity of Novel Perovskite Catalysts. *Catalysts* **2020**, *10*, 582. [CrossRef]

76. Hongmanorom, P.; Ashok, J.; Das, S.; Dewangan, N.; Bian, Z.; Mitchell, G.; Xi, S.; Borgna, A.; Kawi, S. Zr–Ce-incorporated Ni/SBA-15 catalyst for high-temperature water gas shift reaction: Methane suppression by incorporated Zr and Ce. *J. Catal.* **2020**, *387*, 47–61. [CrossRef]

77. Sadat Maboudi, N.; Meshkani, F.; Rezaei, M. Effect of mesoporous nanocrystalline supports on the performance of the Ni-Cu catalysts in the high-temperature water-gas shift reaction. *J. Energy Inst.* **2021**, *96*, 75–89. [CrossRef]

78. Pei, Q.; Qiu, G.; Yu, Y.; Wang, J.; Chen Tan, K.; Guo, J.; Liu, L.; Cao, H.; He, T.; Chen, P. Fabrication of More Oxygen Vacancies and Depression of Encapsulation for Superior Catalysis in the Water−Gas Shift Reaction. *J. Phys. Chem. Lett.* **2021**, *12*, 10646–10653. [CrossRef] [PubMed]

79. Pei, Q.; He, T.; Yu, Y.; Jing, Z.; Wang, J.; Chen Tan, K.; Guo, J.; Liu, L.; Cao, H.; Chen, P. Fabrication of oxygen vacancies through assembling an amorphous titanate overlayer on titanium oxide for a catalytic water–gas shift reaction. *J. Mater. Chem. A* **2021**, *9*, 2784. [CrossRef]

80. Li, Y.-C.; Li, X.-S.; Zhu, B.; Zhu, A.-M. Boosting low-temperature water gas shift reaction over Au/TiO$_2$ nanocatalyst activated by oxygen plasma. *Chem. Eng. J.* **2022**, *430*, 133013. [CrossRef]

81. Shi, J.; Li, H.; Genest, A.; Zhao, W.; Qi, P.; Wang, T.; Rupprechter, G. High-performance water gas shift induced by asymmetric oxygen vacancies: Gold clusters supported by ceria-praseodymia mixed oxides. *Appl. Catal. B-Environ.* **2022**, *301*, 120789. [CrossRef]

82. Meng, Y.; Chen, Y.; Zhou, X.; Pan, G.; Xia, S. Experimental and theoretical investigations into the activity and mechanism of the water-gas shift reaction catalyzed by Au nanoparticles supported on ZneAl/Cr/Fe layered double hydroxides. *Int. J. Hydrog. Energy* **2020**, *45*, 464–476. [CrossRef]

83. Gabrovska, M.; Ivanov, I.; Nikolova, D.; Kovacheva, D.; Tabakova, T. Hydrogen production via water-gas shift reaction over gold supported on Ni-based layered double hydroxides. *Int. J. Hydrog. Energy* **2021**, *46*, 458–473. [CrossRef]

84. Gabrovska, M.; Ivanov, I.; Nikolova, D.; Krstić, J.; Venezia, A.M.; Crişan, D.; Crişan, M.; Tenchev, K.; Idakiev, V.; Tabakova, T. Improved Water–Gas Shift Performance of Au/NiAl LDHs Nanostructured Catalysts via CeO$_2$ Addition. *Nanomaterials* **2021**, *11*, 366. [CrossRef] [PubMed]

85. Santos de Oliveira, C.; Teixeira Neto, E.; Odone Mazali, I. Stabilization and Au sintering prevention promoted by ZnO in CeOx–ZnO porous nanorods decorated with Au nanoparticles in the catalysis of the water-gas shift (WGS) reaction. *J. Alloys Compd.* **2021**, *892*, 162179. [CrossRef]

86. Pastor-Pérez, L.; Ramos-Fernández, E.V.; Sepúlveda-Escribano, A. Effect of the CeO$_2$ synthesis method on the behaviour of Pt/CeO$_2$ catalysis for the water-gas shift reaction. *Int. J. Hydrog. Energy* **2019**, *44*, 21837–21846. [CrossRef]

87. Li, Y.; Kottwitz, M.; Vincent, J.L.; Enright, M.J.; Liu, Z.; Zhang, L.; Huang, J.; Senanayake, S.D.; Yang, W.-C.D.; Crozier, P.A.; et al. Dynamic structure of active sites in ceria-supported Pt catalysts for the water gas shift reaction. *Nat. Commun.* **2021**, *12*, 914. [CrossRef] [PubMed]

88. Gorlova, A.; Zadesenets, A.; Filatov, E.; Simonov, P.; Korenev, S.; Stonkus, O.; Sobyanin, V.; Snytnikov, P.; Potemkin, D. Pt-Fe nanoalloy: Structure evolution study and catalytic properties in water gas shift reaction. *Mater. Res. Bull.* **2022**, *149*, 111727. [CrossRef]

89. Yuan, K.; Sun, X.-C.; Yin, H.-J.; Zhou, L.; Liu, H.-C.; Yan, C.-H.; Zhang, Y.W. Boosting the water gas shift reaction on Pt/CeO$_2$-based nanocatalysts by compositional modification: Support doping versus bimetallic alloying. *J. Energy Chem.* **2022**, *67*, 241–249. [CrossRef]

90. Palma, V.; Gallucci, F.; Pullumbi, P.; Ruocco, C.; Meloni, E.; Martino, M. Pt/Re/CeO$_2$ Based Catalysts for CO-Water–Gas Shift Reaction: From Powders to Structured Catalyst. *Catalysts* **2020**, *10*, 564. [CrossRef]

91. Palma, V.; Pisano, D.; Martino, M. Structured noble metal-based catalysts for the WGS process intensification. *Int. J. Hydrog. Energy* **2018**, *43*, 11745–11754. [CrossRef]

92. García-Moncada, N.; Groppi, G.; Beretta, A.; Romero-Sarria, F.; Odriozola, J.A. Metal Micro-Monoliths for the Kinetic Study and the Intensification of the Water Gas Shift Reaction. *Catalysts* **2018**, *8*, 594. [CrossRef]

93. Palma, V.; Pisano, D.; Martino, M. Comparative Study Between Aluminum Monolith and Foam as Carriers for The Intensification of The CO Water Gas Shift Process. *Catalysts* **2018**, *8*, 489. [CrossRef]

94. Palma, V.; Goodall, R.; Thompson, A.; Ruocco, C.; Renda, S.; Leach, R.; Martino, M. Ceria-coated replicated aluminium sponges as catalysts for the CO-water gas shift process. *Int. J. Hydrog. Energy* **2021**, *46*, 12158–12168. [CrossRef]

95. Meng, L.; Ovalle-Encinia, O.; Lin, J.Y.S. Catalyst-Free Ceramic−Carbonate Dual-Phase Membrane Reactors for High-Temperature Water Gas Shift: A Simulation Study. *Ind. Eng. Chem. Res.* **2021**, *60*, 3581–3588. [CrossRef]

96. Sakakura, T.; Choi, J.-C.; Yasuda, H. Transformation of carbon dioxide. *Chem. Rev.* **2007**, *107*, 2365–2387. [PubMed]

97. Song, Q.-W.; Zhou, Z.-H.; He, L.-N. Efficient, selective and sustainable catalysis of carbon dioxide. *Green Chem.* **2017**, *19*, 3707. [CrossRef]

98. Hepburn, C.; Adlen, E.; Beddington, J.; Carter, E.A.; Fuss, S.; Mac Dowell, N.; Minx, J.C.; Smith, P.; Williams, C.K. The technological and economic prospects for CO_2 utilization and removal. *Nature* **2019**, *575*, 87–97.

99. Liang, J.; Wu, Q.; Huang, Y.B.; Cao, R. Reticular frameworks and their derived materials for CO_2 conversion by thermo catalysis. *Energy Chem.* **2021**, *3*, 100064. [CrossRef]

100. Shah, H.-U.R.; Ahmad, K.; Bashir, M.S.; Shah, S.S.A.; Najam, T.; Ashfaq, M. Metal organic frameworks for efficient catalytic conversion of CO_2 and CO into applied products. *Mol. Catal.* **2022**, *517*, 112055. [CrossRef]

101. Ali, S.S.; Tabassum, N. A review on CO_2 hydrogenation to ethanol: Reaction mechanism and experimental studies. *J. Environ. Chem. Eng.* **2022**, *10*, 106962. [CrossRef]

102. Grice, K.A. Carbon dioxide reduction with homogenous early transition metal complexes: Opportunities and challenges for developing CO_2 catalysis. *Coord. Chem. Rev.* **2017**, *336*, 78–95.

103. Sordakis, K.; Tang, C.; Vogt, L.K.; Junge, H.; Dyson, P.J.; Beller, M.; Laurenczy, G. Homogeneous catalysis for sustainable hydrogen storage in formic acid and alcohols. *Chem. Rev.* **2018**, *118*, 372–433.

104. Yaashikaa, P.R.; Kumar, P.S.; Varjani, S.J.; Saravanan, A. A review on photochemical, biochemical and electrochemical transformation of CO_2 into value-added products. *J. CO2 Util.* **2019**, *33*, 131–147.

105. Ojelade, O.A.; Zaman, S.F. A review on CO_2 hydrogenation to lower olefins: Understanding the structure-property relationships in heterogeneous catalytic systems. *J. CO2 Util.* **2021**, *47*, 101506. [CrossRef]

106. De, S.; Dokania, A.; Ramirez, A.; Gascon, J. Advances in the design of heterogeneous catalysts and thermocatalytic processes for CO_2 utilization. *ACS Catal.* **2020**, *10*, 14147–14185.

107. Perazio, A.; Lowe, G.; Gobetto, R.; Bonin, J.; Robert, M. Light-driven catalytic conversion of CO_2 with heterogenized molecular catalysts based on fourth period transition metals. *Coord. Chem. Rev.* **2021**, *443*, 214018. [CrossRef]

108. Xie, B.; Lovell, E.; Hao Tan, T.; Jantarang, S.; Yu, M.; Scott, J.; Amal, R. Emerging material engineering strategies for amplifying photothermal heterogeneous CO_2 catalysis. *J. Energy Chem.* **2021**, *59*, 108–125. [CrossRef]

109. Chen, Z.; Wang, X.; Liu, L. Electrochemical Reduction of Carbon Dioxide to Value-Added Products: The Electrocatalyst and Microbial Electrosynthesis. *Chem. Rec.* **2019**, *19*, 1272–1282.

110. Palma, V.; Cortese, M.; Renda, S.; Ruocco, C.; Martino, M.; Meloni, E. A review about the recent advances in selected nonthermal plasma assisted solid–gas phase chemical processes. *Nanomaterials* **2020**, *10*, 1596. [CrossRef]

111. Garba, M.D.; Usman, M.; Khan, S.; Shehzad, F.; Galadima, A.; Fahad Ehsan, M.; Ghanem, A.S.; Humayun, M. CO_2 towards fuels: A review of catalytic conversion of carbon dioxide to hydrocarbons. *J. Environ. Chem. Eng.* **2021**, *9*, 104756. [CrossRef]

112. Li, Z.; Wang, J.; Qu, Y.; Liu, H.; Tang, C.; Miao, S.; Feng, Z.; An, H.; Li, C. Highly selective conversion of carbon dioxide to lower olefins. *ACS Catal.* **2017**, *7*, 8544–8548.

113. Tian, H.; He, H.; Jiao, J.; Zha, F.; Guo, X.; Tang, X.; Chang, Y. Tandem catalysts composed of different morphology HZSM-5 and metal oxides for CO_2 hydrogenation to aromatics. *Fuel* **2022**, *314*, 123119. [CrossRef]

114. Zhou, X.; Su, T.; Jiang, Y.; Qin, Z.; Ji, H.; Guo, Z. CuO-Fe_2O_3-CeO_2/HZSM-5 bifunctional catalyst hydrogenated CO_2 for enhanced dimethyl ether synthesis. *Chem. Eng. Sci.* **2016**, *153*, 10–20.

115. Wang, P.; Zha, F.; Yao, L.; Chang, Y. Synthesis of light olefins from CO_2 hydrogenation over (CuO-ZnO)-kaolin/SAPO-34 molecular sieves. *Appl. Clay Sci.* **2018**, *163*, 249–256.

116. Alvarez, A.; Bansode, A.; Urakawa, A.; Bavykina, A.V.; Wezendonk, T.A.; Makkee, M.; Gascon, J.; Kapteijn, F. Challenges in the greener production of Formates/Formic acid, methanol, and DME by heterogeneously catalyzed CO_2 hydrogenation processes. *Chem. Rev.* **2017**, *117*, 9804–9838. [CrossRef] [PubMed]

117. Yarulina, I.; De Wispelaere, K.; Bailleul, S.; Goetze, J.; Radersma, M.; Abou-Hamad, E.; Vollmer, I.; Goesten, M.; Mezari, B.; Hensen, E.J.M.; et al. Structure–performance descriptors and the role of Lewis acidity in the methanol-to-propylene process. *Nat. Chem.* **2018**, *10*, 804–812. [CrossRef]

118. Chowdhury, A.D.; Houben, K.; Whiting, G.T.; Mokhtar, M.; Asiri, A.M.; Al-Thabaiti, S.A.; Basahel, S.N.; Baldus, M.; Weckhuysen, B.M. Initial carbon–Carbon bond formation during the early stages of the methanol-to-Olefin process proven by zeolite-trapped acetate and methyl acetate. *Angew. Chem. Int.* **2016**, *55*, 15840–15845. [CrossRef]

119. Cai, D.; Wang, Q.; Jia, Z.; Ma, Y.; Cui, Y.; Muhammad, U.; Wang, Y.; Qian, W.; Wei, F. Equilibrium analysis of methylbenzene intermediates for a methanol-to-olefins process. *Catal. Sci. Technol.* **2016**, *6*, 1297–1301. [CrossRef]

120. Yarulina, I.; Chowdhury, A.D.; Meirer, F.; Weckhuysen, B.M.; Gascon, J. Recent trends and fundamental insights in the methanol-to-hydrocarbons process. *Nat. Catal.* **2018**, *1*, 398–411. [CrossRef]

121. Zhu, J.; Li, Y.; Muhammad, U.; Wang, D.; Wang, Y. Effect of alkene co-feed on the MTO reactions over SAPO-34. *Chem. Eng. J.* **2017**, *316*, 187–195. [CrossRef]

122. Usman, M.; Zhu, J.; Chuiyang, K.; Arslan, M.T.; Khan, A.; Galadima, A.; Muraza, O.; Khan, I.; Helal, A.; Al-Maythalony, B.A.; et al. Propene adsorption-chemisorption behaviors on H-SAPO-34 zeolite catalysts at different temperatures. *Catalysts* **2019**, *9*, 919.

123. Tada, S.; Kinoshita, H.; Ochiai, N.; Chokkalingam, A.; Hu, P.; Yamauchi, N.; Kobayashi, Y.; Iyoki, K. Search for solid acid catalysts aiming at the development of bifunctional tandem catalysts for the one-pass synthesis of lower olefins via CO_2 hydrogenation. *Int. J. Hydrog. Energy* **2021**, *46*, 36721–36730. [CrossRef]

124. Tong, M.; Chizema, L.G.; Chang, X.; Hondo, E.; Dai, L.; Zeng, Y.; Zeng, C.; Ahmad, H.; Yang, R.; Lu, P. Tandem catalysis over tailored ZnO-ZrO_2/MnSAPO-34 composite catalyst for enhanced light olefins selectivity in CO_2 hydrogenation. *Microporous Mesoporous Mater.* **2021**, *320*, 111105. [CrossRef]

125. Mou, J.; Fan, X.; Liu, F.; Wang, X.; Zhao, T.; Chen, P.; Li, Z.; Yang, C.; Cao, J. CO_2 hydrogenation to lower olefins over Mn_2O_3-ZnO/SAPO-34 tandem catalysts. *Chem. Eng. J.* **2021**, *421*, 129978. [CrossRef]

126. Dorner, R.W.; Hardy, D.R.; Williams, F.W.; Willauer, H.D. Heterogeneous catalytic CO_2 conversion to value-added hydrocarbons. *Energy Environ. Sci.* **2010**, *3*, 884–890. [CrossRef]

127. Smith, Z.P.; Bachman, J.E.; Li, T.; Gludovatz, B.; Kusuma, V.A.; Xu, T.; Hopkinson, D.P.; Ritchie, R.O.; Long, J.R. Increasing M2(dobdc) loading in selective mixed-matrix membranes: A rubber toughening approach. *Chem. Mater.* **2018**, *30*, 1484–1495. [CrossRef]

128. Batchu, R.; Galvita, V.V.; Alexopoulos, K.; Van der Borght, K.; Poelman, H.; Reyniers, M.-F.; Marin, G.B. Role of intermediates in reaction pathways from ethene to hydrocarbons over H-ZSM-5. *Appl. Catal. A Gen.* **2017**, *538*, 207–220. [CrossRef]

129. Kotrel, S.; Knozinger, H.; Gates, B.C. The Haag–Dessau mechanism of protolytic cracking of alkanes. *Microporous Mesoporous Mater.* **2000**, *35–36*, 11–20. [CrossRef]

130. Sartipi, S.; Makkee, M.; Kapteijn, F.; Gascon, J. Catalysis engineering of bifunctional solids for the one-step synthesis of liquid fuels from syngas: A review. *Catal. Sci. Technol.* **2014**, *4*, 893–907. [CrossRef]

131. Hagen, A.; Roessner, F. Ethane to aromatic hydrocarbons: Past, present, Future. *Catal. Rev.* **2000**, *42*, 403–437. [CrossRef]

132. Joshi, Y.V.; Thomson, K.T. Brønsted Acid Catalyzed Cyclization of C7 and C8 Dienes in HZSM-5: A Hybrid QM/MM Study and Comparison with C6 Diene Cyclization. *J. Phys. Chem. C* **2008**, *112*, 12825–12833. [CrossRef]

133. Tabor, E.; Bernauer, M.; Wichterlova, B.; Dedecek, J. Enhancement of propene oligomerization and aromatization by proximate protons in zeolites; FTIR study of the reaction pathway in ZSM-5. *Catal. Sci. Technol.* **2019**, *9*, 4262–4275. [CrossRef]

134. Zhang, Z.; Huang, G.; Tang, X.; Yin, H.; Kang, J.; Zhang, Q.; Wang, Y. Zn and Na promoted Fe catalysts for sustainable production of high-valued olefins by CO_2 hydrogenation. *Fuel* **2022**, *309*, 122105. [CrossRef]

135. Sun, Z.; Chen, X.; Lu, F.; Zhou, L.; Zhang, Y. Effect of Rb promoter on Fe_3O_4 microsphere catalyst for CO_2 hydrogenation to light olefins. *Catal. Commun.* **2022**, *162*, 106387. [CrossRef]

136. Zhang, Z.; Liu, Y.; Jia, L.; Sun, C.; Chen, B.; Liu, R.; Tan, Y.; Tu, W. Effects of the reducing gas atmosphere on performance of FeCeNa catalyst for the hydrogenation of CO_2 to olefins. *Chem. Eng. J.* **2022**, *428*, 131388. [CrossRef]

137. Lino, A.V.P.; Assaf, E.M.; Assaf, J.M. Production of light hydrocarbons at atmospheric pressure from CO_2 hydrogenation using $Ce_xZr_{(1-x)}O_2$ iron-based catalysts. *J. CO2 Util.* **2022**, *55*, 101805. [CrossRef]

138. Al-Zakwani, S.S.; Maroufmashat, A.; Mazouz, A.; Fowler, M.; Elkamel, A. Allocation of Ontario's Surplus Electricity to Different Power-to-Gas Applications. *Energies* **2019**, *12*, 2675.

139. Castellani, B.; Gambelli, A.M.; Morini, E.; Nastasi, B.; Presciutti, A.; Filipponi, M.; Nicolini, A.; Rossi, F. Experimental Investigation on CO2 Methanation Process for Solar Energy Storage Compared to CO_2-Based Methanol Synthesis. *Energies* **2017**, *10*, 855. [CrossRef]

140. Sterner, M.; Specht, M. Power-to-Gas and Power-to-X–The Hystory and Results of Developing a New Storage Concept. *Energies* **2021**, *14*, 6594.

141. Garbarino, G.; Pugliese, F.; Cavattoni, T.; Busca, G.; Costamagna, P. A Study on CO_2 Methanation and Steam Methane Reforming over Commercial Ni/Calcium Aluminate Catalysts. *Energies* **2020**, *13*, 2792. [CrossRef]

142. Rozzi, E.; Minuto, F.D.; Lanzini, A.; Leone, P. Green Synthetic Fuels: Renewable Routes for the Conversion of Non-Fossil Feedstocks into Gaseous Fuels and Their End Uses. *Energies* **2020**, *13*, 420. [CrossRef]

143. Cao, H.; Wang, W.; Cui, T.; Wang, H.; Zhu, G.; Ren, X. Enhancing CO_2 Hydrogenation to Methane by Ni-Based Catalyst with V Species Using 3D-mesoporous KIT-6 as Support. *Energies* **2020**, *13*, 2235. [CrossRef]

144. Tsiotsias, A.I.; Charisiou, N.D.; Yentekakis, I.V.; Goula, M.A. Bimetallic Ni-based catalysts for CO_2 methanation: A review. *Nanomaterials* **2021**, *11*, 28. [CrossRef]

145. Renda, S.; Ricca, A.; Palma, V. Study of the effect of noble metal promotion in Ni-based catalyst for the Sabatier reaction. *Int. J. Hydrog. Energy* **2020**, *46*, 12117–12127. [CrossRef]

146. Ghaib, K.; Nitz, K.; Ben-Fares, F.Z. Chemical methanation of CO_2: A review. *ChemBioEng Rev.* **2016**, *3*, 266–275. [CrossRef]

147. Di Stasi, C.; Renda, S.; Greco, G.; González, B.; Palma, V.; Manyà, J.J. Wheat-straw-derived activated biochar as a renewable support of Ni-CeO_2 catalysts for CO_2 methanation. *Sustainability* **2021**, *13*, 8939. [CrossRef]

148. Frontera, P.; Macario, A.; Ferraro, M.; Antonucci, P.L. Supported catalysts for CO_2 methanation: A review. *Catalysts* **2017**, *7*, 59. [CrossRef]

149. Lee, W.J.; Li, C.; Prajitno, H.; Yoo, J.; Patel, J.; Yang, Y.; Lim, S. Recent trend in thermal catalytic low temperature CO_2 methanation: A critical review. *Catal. Today* **2021**, *368*, 2–19. [CrossRef]

150. Ashok, J.; Pati, S.; Hongmanorom, P.; Tianxi, Z.; Junmei, C.; Kawi, S. A review of recent catalyst advances in CO_2 methanation processes. *Catal. Today* **2020**, *356*, 471–489. [CrossRef]

151. Fan, W.K.; Tahir, M. Recent trends in developments of active metals and heterogenous materials for catalytic CO2 hydrogenation to renewable methane: A review. *J. Environ. Chem. Eng.* **2021**, *9*, 105460.

152. Huynh, H.L.; Yu, Z. CO_2 Methanation on Hydrotalcite-Derived Catalysts and Structured Reactors: A Review. *Energy Technol.* **2020**, *8*, 1901475. [CrossRef]

153. Huynh, H.L.; Tucho, W.M.; Shen, Q.; Yu, Z. Bed packing configuration and hot-spot utilization for low-temperature CO_2 methanation on monolithic reactor. *Chem. Eng. J.* **2022**, *428*, 131106.

154. García-Moncada, N.; Navarro, J.C.; Odriozola, J.A.; Lefferts, L.; Faria, J.A. Enhanced catalytic activity and stability of nanoshaped Ni/CeO$_2$ for CO$_2$ methanation in micro-monoliths. *Catal. Today* **2022**, *383*, 205–215. [CrossRef]

155. Navarro, J.C.; Centeno, M.A.; Laguna, O.H.; Odriozola, J.A. Ru–Ni/MgAl$_2$O$_4$ structured catalyst for CO$_2$ methanation. *Renew. Energy* **2020**, *161*, 120–132. [CrossRef]

156. Ratchahat, S.; Sudoh, M.; Suzuki, Y.; Kawasaki, W.; Watanabe, R.; Fukuhara, C. Development of a powerful CO2 methanation process using a structured Ni/CeO$_2$ catalyst. *J. CO2 Util.* **2018**, *24*, 210–219. [CrossRef]

157. Vita, A.; Italiano, C.; Pino, L.; Laganà, M.; Ferraro, M.; Antonucci, V. High-temperature CO$_2$ methanation over structured Ni/GDC catalysts: Performance and scale-up for Power-to-Gas application. *Fuel Process. Technol.* **2020**, *202*, 106365. [CrossRef]

158. Ricca, A.; Truda, L.; Palma, V. Study of the role of chemical support and structured carrier on the CO$_2$ methanation reaction. *Chem. Eng. J.* **2019**, *377*, 120461. [CrossRef]

159. Cimino, S.; Cepollaro, E.M.; Lisi, L.; Fasolin, S.; Musiani, M.; Vázquez-Gómez, L. Ru/ce/ni metal foams as structured catalysts for the methanation of CO$_2$. *Catalysts* **2021**, *11*, 13. [CrossRef]

160. Italiano, C.; Ferrante, G.D.; Pino, L.; Laganà, M.; Ferrato, M.; Antonucci, V.; Vita, A. Silicon carbide and alumina open-cell foams activated by Ni/CeO$_2$-ZrO$_2$ catalyst for CO$_2$ methanation in a heat-exchanger reactor. *Chem. Eng. J.* **2022**, *434*, 134685. [CrossRef]

161. Sánchez, A.; Milt, V.G.; Miró, E.E.; Güttel, R. Impact of heat transport properties and configuration of ceramic fibrous catalyst structures for CO$_2$ methanation: A simulation study. *J. Environ. Chem. Eng.* **2022**, *10*, 107148. [CrossRef]

162. Danaci, S.; Protasova, L.; Lefevere, J.; Bedel, L.; Guilet, R.; Marty, P. Efficient CO$_2$ methanation over Ni/Al$_2$O$_3$ coated structured catalysts. *Catal. Today* **2016**, *273*, 234–243. [CrossRef]

163. Danaci, S.; Protasova, L.; Snijkers, F.; Bouwen, W.; Bengaouer, A.; Marty, P. Innovative 3D-manufacture of structured copper supports post-coated with catalytic material for CO$_2$ methanation. *Chem. Eng. Process.—Process Intensif.* **2018**, *127*, 168–177. [CrossRef]

164. Fuentes, I.; Gracia, F. Fluid dynamic analytical model of CO$_2$ methanation in a microreactor with potential application in Power-to-Gas technology. *Chem. Eng. Sci.* **2022**, *251*, 117465, in press. [CrossRef]

165. Catarina Faria, A.; Miguel, C.V.; Madeira, L.M. Thermodynamic analysis of the CO$_2$ methanation reaction with in situ water removal for biogas upgrading. *J. CO2 Util.* **2018**, *26*, 271–280. [CrossRef]

166. Ohya, H.; Fun, J.; Kawamura, H.; Itoh, K.; Ohashi, H.; Aihara, M.; Tanisho, S.; Negishi, Y. Methanation of carbon dioxide by using membrane reactor integrated with water vapor permselective membrane and its analysis. *J. Memb. Sci.* **1997**, *131*, 237–247. [CrossRef]

167. Catarina Faria, A.; Miguel, C.V.; Rodrigues, A.E.; Madeira, L.M. Modeling and Simulation of a Steam-Selective Membrane Reactor for Enhanced CO$_2$ Methanation. *Ind. Eng. Chem. Res.* **2020**, *59*, 16170–16184. [CrossRef]

168. Liu, Z.; Bian, Z.; Wang, Z.; Jiang, B. A CFD study on the performance of CO$_2$ methanation in a water-permeable membrane reactor system. *React. Chem. Eng.* **2022**, *7*, 450–459. [CrossRef]

169. Miyamoto, M.; Hayakawa, R.; Makino, Y.; Oumi, Y.; Uemiya, S.; Asanuma, M. CO$_2$ methanation combined with NH$_3$ decomposition by in situ H$_2$ separation using a Pd membrane reactor. *Int. J. Hydrog. Energy* **2014**, *39*, 10154–10160. [CrossRef]

170. Bian, Z.; Xia, H.; Zhong, W.; Jiang, B.; Yu, Y.; Wang, Z.; Yu, K. CFD simulation on hydrogen-membrane reactor integrating cyclohexane dehydrogenation and CO$_2$ methanation reactions: A conceptual study. *Energy Convers. Manag.* **2021**, *235*, 113989. [CrossRef]

171. Bacariza, M.C.; Biset-Peiró, M.; Graça, I.; Guilera, J.; Morante, J.; Lopes, J.M.; Andreu, T.; Henriques, C. DBD plasma-assisted CO$_2$ methanation using zeolite-based catalysts: Structure composition-reactivity approach and effect of Ce as promoter. *J. CO2 Util.* **2018**, *26*, 202–211. [CrossRef]

172. Ahmad, F.; Lovell, E.C.; Masood, H.; Cullen, P.J.; Ostrikov, K.K.; Scott, J.A.; Amal, R. Low-Temperature CO$_2$ Methanation: Synergistic Effects in Plasma-Ni Hybrid Catalytic System. *ACS Sustain. Chem. Eng.* **2020**, *8*, 1888–1898. [CrossRef]

173. Wierzbicki, D.; Moreno, M.V.; Ognier, S.; Motak, M.; Grzybek, T.; Da Costa, P.; Gálvez, M.E. Ni-Fe layered double hydroxide derived catalysts for non-plasma and DBD plasma-assisted CO$_2$ methanation. *Int. J. Hydrog. Energy* **2020**, *45*, 10423–10432. [CrossRef]

174. Biset-Peiró, M.; Mey, R.; Guilera, J.; Andreu, T. Adiabatic plasma-catalytic reactor configuration: Energy efficiency enhancement by plasma and thermal synergies on CO$_2$ methanation. *Chem. Eng. J.* **2020**, *393*, 124786. [CrossRef]

175. Gao, Y.; Dou, L.; Zhang, S.; Zong, L.; Pan, J.; Hu, X.; Sun, H.; Ostrikov, K.; Shao, T. Coupling bimetallic Ni-Fe catalysts and nanosecond pulsed plasma for synergistic low-temperature CO$_2$ methanation. *Chem. Eng. J.* **2021**, *420*, 127693. [CrossRef]

176. Gao, W.; Chen, H. Mechanochemical Synthesis of Ni−Y/CeO$_2$ Catalyst for Nonthermal Plasma Catalytic CO$_2$ Methanation. *Ind. Eng. Chem. Res.* **2022**, *61*, 1666–1674. [CrossRef]